

Spherical squirmers: models for swimming micro-organisms

T. J. PEDLEY*

*Department of Applied Mathematics and Theoretical Physics, Centre for Mathematical Sciences,
University of Cambridge, Wilberforce Road, Cambridge CB3 0WA, UK*

*Corresponding author: tjp3@cam.ac.uk

[Received on 18 March 2016]

In 1952, Lighthill introduced the simplest possible model of a swimming micro-organism of finite size, intended as a model of a single-celled protozoan covered in beating cilia. The model consisted of a sphere, on the surface of which material points undergo small-amplitude oscillations. In 1971, Lighthill's student, John Blake, completed the calculations and applied the theory to various species of ciliate. Subsequently we, and many others, have used the even simpler (though less realistic) model of a steady squirmer, a sphere whose surface moves tangentially with time-independent velocity. In this article we survey:

- low-Reynolds-number locomotion, nutrient uptake and optimisation of individual squirmers;
- hydrodynamic interactions between pairs of steady squirmers and their influence on clustering, self-diffusion and rheology in suspensions of squirmers, including the effect of being bottom-heavy;
- measurements and modelling of metachronal waves in *Volvox*, the only truly spherical multi-celled organism, culminating in predictions of the mean swimming speed and angular velocity of free-swimming *Volvox*. The predictions are compared with experiment.

Keywords: low-Reynolds-number hydrodynamics; microorganism locomotion; collective behaviour; *Volvox*.

1. Introduction

Swimming micro-organisms are everywhere: inside people (sperm, gut bacteria) and outside (algae and bacteria in bioreactors, lakes and oceans). This article is concerned with modelling the fluid dynamics of micro-organism swimming, from an applied mathematician's perspective. The Reynolds number of swimming micro-organisms is invariably small, so the fluid dynamics will be governed by the linear Stokes equations, as long as the fluid in which the organisms are swimming is Newtonian. However, micro-organisms come in a great variety of geometries and swimming modes (Fig. 1): typical bacteria have round or elongated cell bodies (body length $\sim 2 \mu\text{m}$) with several long ($\sim 10 \mu\text{m}$) helical flagella that are rigid except for a compliant zone near the base, and which bundle together and rotate to provide a corkscrew-like thrust from behind the cell body (Berg, 2004); most sperm have a compact head with a long ($\sim 40 \mu\text{m}$ in humans) flexible flagellum behind, along which bending waves propagate to produce thrust (Brennen & Winet, 1977); some algal cells (body length 5–10 μm) have two flagella, and normally pull themselves through the water using breaststroke-like motions (Rüffer & Nultsch, 1985); many protists, such as *Opalina* and *Paramecium* (cell length up to 250 μm) are covered with closely-spaced cilia (length $\sim 5 \mu\text{m}$) whose beating is coordinated in the form of a metachronal wave (Fig. 2) (Sleigh, 1962). Effectively, cilia are just short flagella; the transverse structure of the cilia and flagella in all eukaryotes (as opposed to bacteria, which are prokaryotes) is identical, and has been for a billion years, which makes it one of the most highly conserved structures in biology. A review of the above, and other, modes of locomotion would be extremely long and is beyond the scope of this article,

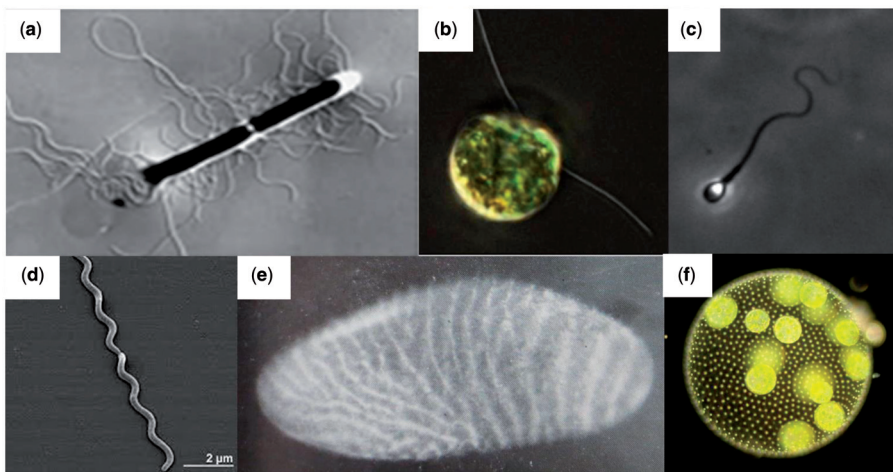


FIG. 1. Examples of swimming micro-organisms. Top row (a) bacterium (*Bacillus subtilis*), (b) biflagellate alga (*Chlamydomonas reinhardtii*), (c) human spermatozoon, (d) spirochete (*Spirochaeta smaragdinae*), (e) *Opalina*, (f) *Volvox carteri*. Sources: (a), (b) and (f) kindly supplied by Prof. Raymond E. Goldstein; (c) kindly supplied by Dr. David J. Smith; (d) from Mavromatis *et al* (2010) (with permission); (e) from Sleigh (1962).

Metachronal waves

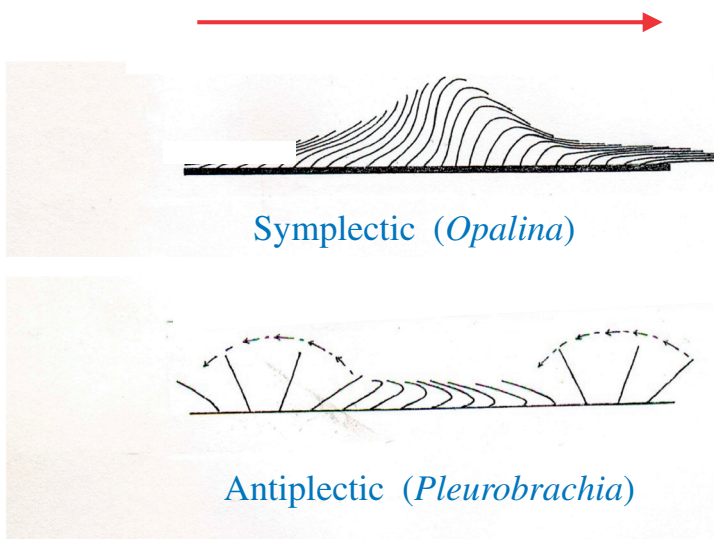


FIG. 2. Sketches of metachronal waves in an array of cilia: (a) Symplectic (wave propagation in same direction as power stroke), as for *Opalina*; (b) antiplectic (wave propagation in opposite direction to power stroke), as for *Pleurobrachia*. From Sleigh (1962).

and anyway there have been excellent recent reviews of low-Reynolds-number swimming by Lauga & Powers (2009) and by Guasto *et al.* (2012).

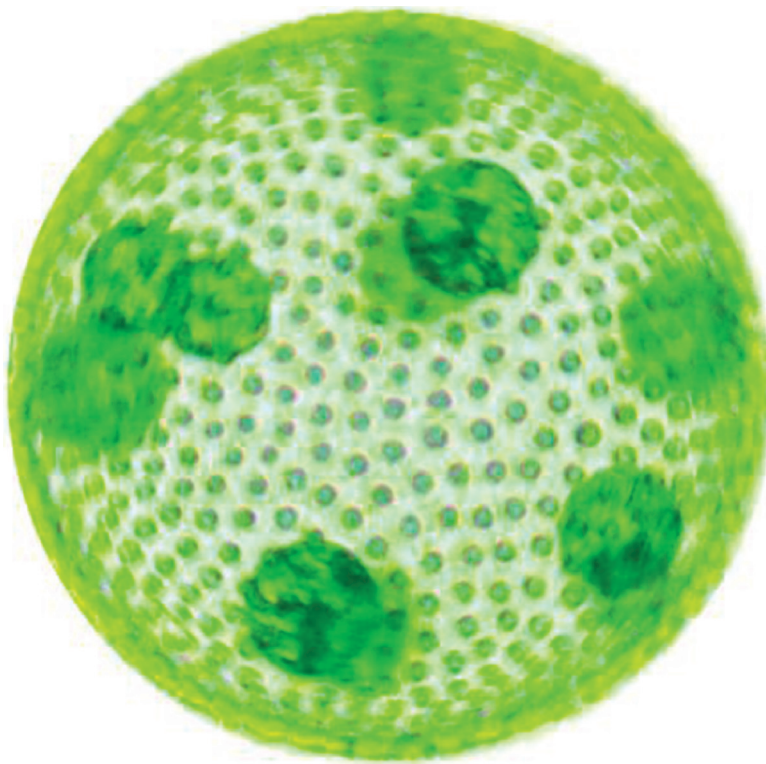


FIG. 3. A colony of *Volvox carteri*. Small green dots are the somatic cells on the outside; large green circles are the daughter colonies on the inside. The photograph is taken from above, as the colony swims upwards towards the camera. From Pedley *et al.* (2016).

A very important type of organism in the context of this article is *Volvox*, which is a genus of algal cells that forms perfectly spherical, free-swimming colonies consisting of up to 50,000 somatic cells on the outside and a number of germ cells, forming the next generation of colonies, on the inside (Fig. 3). The somatic cells are embedded in an extracellular matrix. The colonies are about 0.3% denser than water, and swim upwards in still water, parallel to an axis of symmetry, because the relatively dense interior cells are clustered towards the rear; if the axis were not vertical the colony would experience a gravitational torque that would render it vertical. The colonies are observed to rotate about the axis. Each somatic cell has two flagella and these all beat more or less in planes that are offset from purely meridional planes by an angle of 10°–20°; it is believed that this offset causes the observed rotation. The power stroke of a flagellum's beat is directed towards the rear—i.e. from the ‘north pole’ towards the ‘south pole’—apart from the angular offset. More experimental data on *Volvox* will be given below, where relevant. An excellent review of Volvocine algae and their fluid dynamics has been given by Goldstein (2015).

Finally, as an aside, we may note that not all motile micro-organisms have cilia or flagella: e.g. many species of the intriguing cyanobacterium *Synechococcus* move through still water, at speeds of up to 25 μms^{-1} , but have no observable appendages (e.g. cilia) or deformations of the cell membrane (Waterbury *et al.*, 1985).

The first analysis of the fluid dynamics of low-Reynolds-number propulsion appeared in the early 1950s. In an approach to modelling the propulsion of a long sperm tail, Taylor (1951) showed that an infinite, deformable sheet immersed in a viscous fluid could propel itself to the left by generating small-amplitude transverse waves which propagate to the right. The speed of propulsion U is proportional to the speed of the wave and the square of the amplitude ϵ . The linearity and time-reversibility of the Stokes equations means that there can be no contribution to U from a term linear in ϵ .

An equally idealised model, but for a finite body, was introduced by Lighthill (1952): the *spherical squirmer*. Lighthill considered a sphere with a deformable surface and postulated small-amplitude (ϵ) radial and tangential, axisymmetric and periodic motions of elements of the surface. He showed that the body as a whole could be made to ‘swim’ at a non-zero mean velocity, \bar{U} , again proportional to ϵ^2 . A key constraint, in the absence of inertia, is that the total force on the body must be zero at every instant. Later, Lighthill’s research student Blake (1971) developed the squirmer model further (including correcting some of Lighthill’s analysis) and applied it to the locomotion of ciliates. Here the deformable and stretchable surface of the sphere is thought of as being the envelope of the tips of the cilia as they are beating. The title of Blake’s article: ‘A spherical envelope approach to ciliary propulsion’ shows how the spherical squirmer had already become biologically relevant.

Later, the present author set an exam question (for third year undergraduates) in which an even more idealised version of the spherical squirmer was proposed: there were no radial displacements of the surface, and the tangential velocity was time-independent (Tripos, 1986). Part of the question is reproduced here:

A spherical micro-organism of radius a and mass $\frac{4}{3}\pi a^3 \rho_b$ propels itself through the fluid by secreting and re-absorbing mucus on its surface in such a way that the velocity at its surface is

$$u_r = 0, \quad u_\theta = V \sin \theta [1 + \beta(1 - 5 \cos^2 \theta)] \quad (1.1)$$

in spherical polar co-ordinates with origin fixed at the centre of the sphere. The animal swims, with $\theta = 0$ directed vertically upwards, at velocity U relative to the fluid at infinity. Verify that, with axes fixed in the fluid at infinity, the Stokes stream function ψ takes the form

$$\psi = \left(Ar + \frac{B}{r} \right) \sin^2 \theta + \left(\frac{C}{r} + \frac{D}{r^2} \right) \sin^2 \theta (1 - 5 \cos^2 \theta), \quad (1.2)$$

where A, B, C and D are constants to be found. Calculate U , and show that the animal will move upwards if

$$V > a^2(\rho_b - \rho)g/3\mu. \quad (1.3)$$

This may represent the birth of the *steady squirmer*; I have no knowledge of it being proposed earlier. It should be emphasised that I was (and remain) unaware of any real animal that behaves like this, I had never heard of *Synechococcus*, or even *Volvox*, and the intention was merely to find a simple model for low-Reynolds-number swimming, for which boundary conditions could be precisely specified, but which would still be accessible to students in an examination environment (this last proved to be somewhat optimistic).

Subsequently, the steady squirmer has been used by a number of researchers to shed light on micro-organism swimming, in various contexts such as the effect of swimming on mass transfer, and hydrodynamic interactions between squirmers in a suspension. The first part of this article (Sections 2

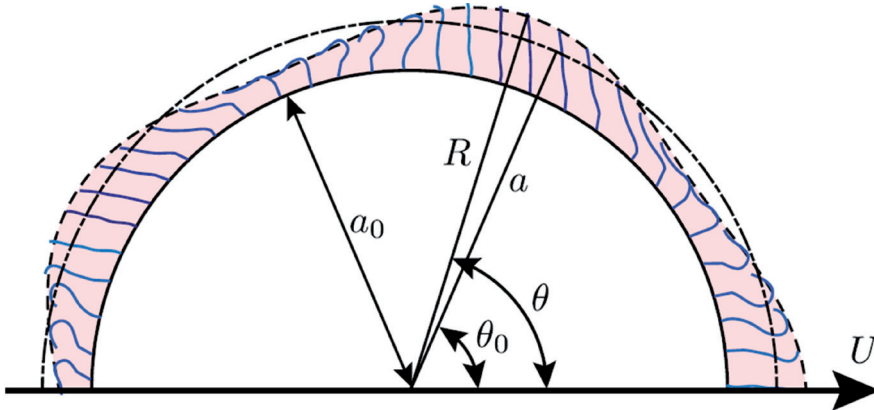


FIG. 4. Schematic diagram of (half of) a spherical *Volvox* colony at one instant in time, with beating flagella and the envelope of flagellar tips. The radius of the extracellular matrix in which the flagella are embedded is a_0 . The mean radius of the envelope is a ; (R, θ) are the coordinates of a surface element whose average position is (a, θ_0) . From Pedley *et al.* (2016).

and 3) will survey much of this work. In the second part (Section 4) we will return to the unsteady squirmer model of Lighthill and Blake which, when suitably extended, proves to be able to predict the mean swimming speed and mean angular velocity of *Volvox*. The difference from earlier work is that the predictions are compared directly with experimental measurements. The swimming of *Volvox* will be described in more detail below, but in a nutshell the flagella of its somatic cells beat in a coordinated way, leading to a metachronal wave at the surface (Brumley *et al.*, 2012), and we use the measured properties of that wave as input to the model. The predictions significantly underestimate both translational and angular velocity (unless the amplitude of the flagellar beating is taken to be about 2.5 times larger than observed, when the predictions and measurements agree rather well); the reason for the underestimate is briefly discussed.

2. The individual steady squirmer

The sphere of radius a is here taken to be neutrally buoyant, so it experiences zero hydrodynamic force. The tangential velocity on its surface, $u_\theta(a, \theta_0)$, is taken to be axisymmetric; we use spherical polar co-ordinates (r, θ_0) fixed at the centre of the sphere (Fig. 4). The velocity field outside the sphere can be represented as an infinite series of eigenfunctions of the Stokes equations (Blake, 1971):

$$u_r(r, \theta_0) = -U \cos \theta_0 + A_0 \frac{a^2}{r^2} P_0 + \frac{2}{3}(A_1 + B_1) \frac{a^3}{r^3} P_1 + \sum_{n=2}^{\infty} \left[\left(\frac{1}{2}n \frac{a^n}{r^n} - \left(\frac{1}{2}n - 1 \right) \frac{a^{n+2}}{r^{n+2}} \right) A_n P_n + \left(\frac{a^{n+2}}{r^{n+2}} - \frac{a^n}{r^n} \right) B_n P_n \right] \quad (2.1a)$$

$$u_\theta(r, \theta_0) = U \sin \theta_0 + \frac{1}{3}(A_1 + B_1) \frac{a^3}{r^3} V_1 + \sum_{n=2}^{\infty} \left[\left(\frac{1}{2}n \frac{a^{n+2}}{r^{n+2}} - \left(\frac{1}{2}n - 1 \right) \frac{a^n}{r^n} \right) B_n V_n + \frac{1}{2}n \left(\frac{1}{2}n - 1 \right) \left(\frac{a^n}{r^n} - \frac{a^{n+2}}{r^{n+2}} \right) A_n V_n \right], \quad (2.1b)$$

where U is the velocity of the fluid at infinity—i.e. the swimming speed of the sphere—and

$$V_n(\cos \theta_0) = \frac{2}{n(n+1)} \sin \theta_0 P'_n(\cos \theta_0); \quad (2.2)$$

P_n are Legendre polynomials. Thus the prescribed velocity on $r = a$ should be expressed in the form

$$u_r(a, \theta_0) = \sum_{n=0}^{\infty} A_n(t) P_n(\cos \theta_0), \quad u_\theta(a, \theta_0) = \sum_{n=1}^{\infty} B_n(t) V_n(\cos \theta_0). \quad (2.3)$$

In this section we will assume that the radial velocity at $r = a$ is zero—i.e. $A_n = 0$ for all n —so that the squirmer remains a pure sphere throughout. The condition that the sphere experiences zero hydrodynamic force requires the Stokeslet term in the above equations to be zero; hence

$$U = \frac{2}{3} B_1. \quad (2.4)$$

A short cut to this formula was achieved by Anderson & Prieve (1991) and independently by Stone & Samuel (1996). They used the reciprocal theorem for Stokes flow to relate the translation and rotation speeds of a deformable body with non-zero surface velocity \mathbf{u}' to the drag and torque on a rigid body of instantaneously identical shape, and derived the following results for a sphere of radius a , surface S :

$$\mathbf{U}(t) = -\frac{1}{4\pi a^2} \int_S \mathbf{u}' dS \quad (2.5a)$$

$$\boldsymbol{\Omega}(t) = -\frac{3}{8\pi a^3} \int_S \mathbf{n} \times \mathbf{u}' dS, \quad (2.5b)$$

where \mathbf{n} is the outward normal to the sphere. From the first of these (2.4) follows. It turns out not to be so simple to use these results for squirmers with non-zero radial deformations, because of the need to calculate the drag to $O(\epsilon^2)$ for the rigid deformed sphere.

For many of the applications to be presented it is convenient to have an easily manageable set of formulae, and many interesting features can be discussed if the series in (2.3) is truncated after only two terms, i.e. $B_n = 0$ for $n > 2$, and

$$u_\theta(a, 0) = \frac{B_1}{3} V_1(\cos \theta_0) + B_2 V_2(\cos \theta_0) = \frac{B_1}{3} \sin \theta_0 + B_2 \sin \theta_0 \cos \theta_0. \quad (2.6)$$

The second term corresponds to a force-dipole, or stresslet. If $B_2 > 0$, the sphere exerts a backwards net force on the fluid at the front (i.e. for $0 < \theta_0 < \pi/2$) and a forwards force at the back, pulling itself through the fluid and ejecting fluid sideways near the ‘equator’. If $B_2 < 0$, the sphere can be thought of as pushing itself through the fluid from behind; fluid is sucked in near the equator. Throughout this article we use the ratio

$$\beta = B_2/B_1 \quad (2.7)$$

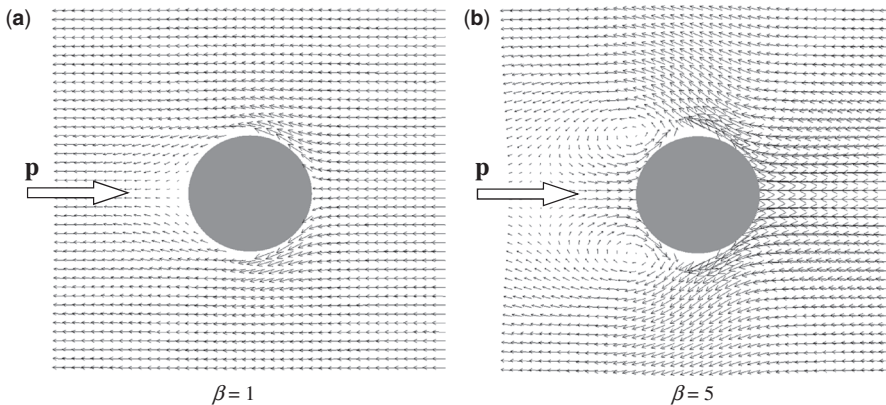


FIG. 5. Velocity vectors in the reference frame moving with the squirmer in direction p . Uniform flow of speed $U = 1$ (dimensionless) coming from the far right. (a) $\beta = 1$, (b) $\beta = 5$. From [Ishikawa et al. \(2008\)](#).

as the parameter that represents the swimming mode: $\beta > 0$ for a puller, $\beta < 0$ for a pusher and $\beta = 0$ for a neutral, or treadmill, swimmer. When $\beta = 0$, the flow field (2.1) is that of a source doublet, or potential dipole. Streamlines for two values of β are shown in Fig. 5. Note that, when $|\beta| > 1$, regions of closed streamlines are formed, behind the sphere for pullers and in front for pushers.

A slight variation of the above model, proposed by [Short et al. \(2006\)](#), is to prescribe the viscous shear stress $\sigma_{r\theta}$ applied to the fluid by the squirmer. For the above velocity field (2.1) with $A_n = 0$, this is equal at $r = a$ to

$$\sigma_{r\theta} = -\frac{\mu}{a} \left[2B_1 V_1(\cos \theta_0) + \sum_{n=2}^{\infty} (2n+1) B_n V_n(\cos \theta_0) \right], \quad (2.8)$$

where μ is the fluid viscosity. If, as has been proposed, the shear stress is taken to be uniform over the surface of the sphere, = F say, then

$$B_1 = \frac{9\pi}{16} F \quad (2.9a)$$

$$B_{2m} = 0, \quad B_{2m+1} = \frac{\pi^2(m+1)}{2m} \left[\Gamma(m+1) \Gamma\left(-m - \frac{1}{2}\right) \right]^{-2} F \quad \text{for } m \geq 1. \quad (2.9b)$$

Note in particular that $B_2 = 0$ so this model has zero stresslet, although it does have some higher order agitation of the surface.

One of the quantities that may have biological relevance is the rate of viscous energy dissipation, and hence the mechanical efficiency of the model organism ([Lighthill, 1975](#)). Calculation of the dissipation, P , for a squirmer with surface velocity (2.3) with $A_n = 0$, gives

$$P = 16\pi\mu a \left[\frac{1}{3} B_1^2 + \sum_{n=2}^{\infty} \frac{1}{n(n+1)} B_n^2 \right]. \quad (2.10)$$

This suggests the possibility of optimization; [Michelin & Lauga \(2010\)](#) have indeed shown that the minimum energy dissipation for a given swimming speed, or equivalently the maximum speed for a given power supply, is given by $B_n = 0$ for all $n > 1$. In other words a neutral swimmer, neither a puller nor a pusher, is the most energetically efficient steady squirmers.

2.1. Nutrient uptake

Whether it is biologically important to be energetically efficient depends on whether an organism can take up a plentiful supply of nutrient from its environment. Mass transport by pure diffusion, to a stationary sphere in a fluid at rest, with nutrient concentration C_∞ far away and with given concentration C_0 on its surface, is given by

$$Q_0 = 4\pi aD(C_\infty - C_0), \quad (2.11)$$

where D is the nutrient diffusivity in the fluid. The question is whether swimming, because of either translation through the fluid or merely stirring of the fluid close to the sphere, can significantly enhance the uptake. Even at small Reynolds number, mass transfer may be enhanced if the Péclet number, $Pe = aU/D$, is not small, and it may not be small since the diffusivities of even small solute molecules are around $10^{-5} \text{ cm}^2 \text{ s}^{-1}$, a thousand times smaller than the kinematic viscosity, ν , of water. For bacteria or single-celled algae, Pe remains less than 1 ([Berg & Purcell, 1977](#)), but for the larger *Volvox* species, with $a \approx 0.1 - 1 \text{ mm}$ and $U \approx 0.1 - 1 \text{ mm s}^{-1}$, Pe can be greater than 100 ([Goldstein, 2015](#)).

Mathematically, the problem is to solve the advection-diffusion equation

$$\mathbf{u} \cdot \nabla C = \frac{1}{Pe} \nabla^2 C, \quad (2.12)$$

where C is the solute concentration and the velocity \mathbf{u} and gradient operator ∇ have been made dimensionless with respect to U and a^{-1} respectively. The boundary condition at infinity is $C \rightarrow C_\infty$ as $r \rightarrow \infty$ (r is also now taken to be non-dimensional). The standard boundary condition on the sphere, as indicated above, is $C = C_0$, a constant, at $r = 1$. However, this may be over-idealised for biological applications, and it is worth also considering another one, e.g. to represent diffusion and uniform consumption within the sphere:

$$\text{at } r = 1, \quad D \frac{\partial C}{\partial r} = \gamma(C - C_{\text{cell}}) = D_C \frac{\partial C_{\text{cell}}}{\partial r} \quad (2.13)$$

and, for $0 \leq r < 1$,

$$\nabla^2 C_{\text{cell}} - \kappa^2 C_{\text{cell}} = 0, \quad (2.14)$$

where C_{cell} is the concentration inside the sphere, κ^2 represents the consumption rate, D_C is the internal diffusivity and γ is a membrane transport coefficient.

The above steady problem was solved by [Magar et al. \(2003\)](#) for both boundary conditions; most of the following results are given for the standard boundary condition. For small Pe the method of matched asymptotic expansions was used, following the analysis of [Acrivos & Taylor \(1962\)](#) for heat transfer to (or from) a rigid sphere pulled through the fluid at constant speed by an external force (e.g. a sedimenting, dense sphere). For larger Pe the problem was solved numerically. The results are given in Fig. 6(a and

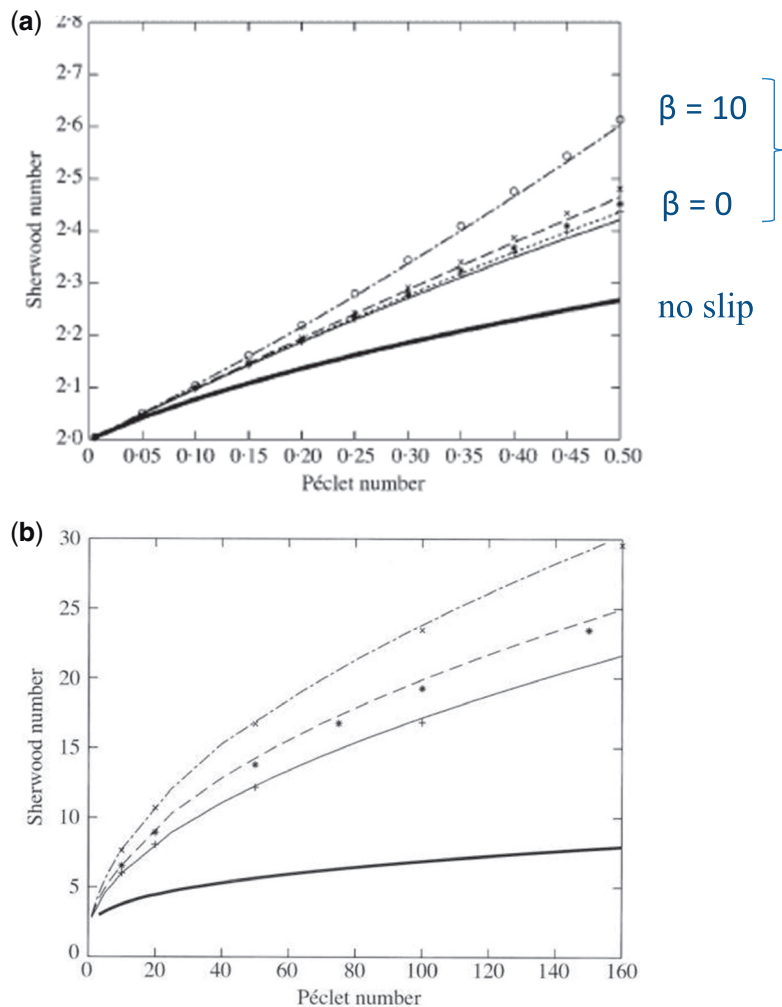


FIG. 6. (a) $2 \times Sh$ versus Pe for Péclet numbers up to 0.5. Thick solid line: numerical results for rigid sphere; thin solid line: $\beta = 1$ analytical; dotted line $\beta = 3$ analytical; dashed line $\beta = 5$ analytical; dash-dot line $\beta = 10$ analytical. Points are corresponding numerical results. (b) As (a) but for larger Pe . All results are numerical. Thick solid line: rigid sphere; thin solid line: $\beta = 0.1$; dashed line: $\beta = 3$; dash-dot line: $\beta = 5$. Points and curves were obtained using two different numerical methods. From Magar *et al.* (2003).

b), as plots of the Sherwood number, Sh , against Pe , for various positive values of β . The Sherwood number is defined as the ratio of the actual nutrient uptake,

$$Q = 2\pi a D \int_0^\pi \left. \frac{\partial C}{\partial r} \right|_{r=1} \sin \theta \, d\theta, \quad (2.15)$$

to the uptake by pure diffusion, Q_0 (2.11). (The values of Sh plotted in Fig. 6 were multiplied by a factor of 2.)

TABLE 1 Comparison of the numerical and asymptotic large Péclet number results for the function $f(\beta)$ (2.16)

β	$f(\beta)$ numerical	$f(\beta)$ asymptotic (i)	$f(\beta)$ asymptotic (ii)	Error
0.1	1.64	1.60		3%
1	1.65	1.60		3%
3	1.89	1.74	2.42	9%
5	2.32	1.95	3.10	19%

It can be seen that, except at very small Pe , the presence of squirming enhances the uptake over that to a rigid sphere translating at the same speed, an effect that increases with both Pe and β . Asymptotic solutions for large Pe can be sought using boundary-layer theory, as was done by Acrivos & Taylor (1962), on the assumption that the concentration remains equal to C_∞ except in a thin layer close to the spherical boundary. The dominant, balancing terms in (2.12) are advection along the boundary and diffusion normal to it. For a rigid sphere, with no slip at the boundary, the longitudinal velocity varies linearly with distance from the boundary, so the boundary-layer thickness, δ , will be proportional to $Pe^{-1/3}$, and the Sherwood number will scale as $Pe^{1/3}$, as $Pe \rightarrow \infty$ (Lighthill, 1950). In the case of a squirmer, the tangential velocity does not go to zero at the boundary, with the consequence that δ should be proportional to $Pe^{-1/2}$ and $Sh \propto Pe^{1/2}$. This is indeed what is found from the numerical solution. If we write

$$Sh \sim f(\beta)Pe^{1/2} \quad (2.16)$$

as $Pe \rightarrow \infty$, the coefficient $f(\beta)$ can be deduced from the computations and is given in Table 1, column 1. However, analytically calculating $f(\beta)$ is not as straightforward as expected, at least for $|\beta| > 1$. The problem lies in the region of closed streamlines remarked on in Fig. 5. In the case of pullers ($\beta > 0$) we certainly expect a thin boundary layer over the front part of the sphere, but only as far as the separation point $\theta = \theta_s$, where $\cos \theta_s = -1/\beta$. Plots of concentration contours for $\beta = 5$ and $Pe = 10$ and 100 are given in Fig. 7, and confirm the presence of the thin boundary layer over the front of the squirmer. Solving the boundary-layer equation for $0 \leq \theta < \theta_s$ is straightforward (Magar *et al.*, 2003) and gives the results in Table 1, column 2. These agree with the numerical results to within 3% (a measure of the error in the numerical solution at large Pe) for $0 < \beta \leq 1$. However, there is a much larger underestimate of $f(\beta)$ for $\beta > 1$. Examination of Fig. 7 indicates why: there is also a thin boundary layer beneath the region of closed streamlines. Solution of the boundary-layer equation in this region, with $C \rightarrow C_\infty$ outside the boundary layer, gives the results in Table 1, column 3, which are now even more gross overestimates of $f(\beta)$. The reason lies in the assumption that $C \rightarrow C_\infty$ outside the boundary layer: in the region of closed streamlines it does not, as can be seen from Fig. 7. But this means that we cannot solve for the large- Pe value of the Sherwood number using boundary-layer theory alone, because although the boundary layer is thin over the rear of the squirmer, there is no way of knowing what the concentration just outside it is without solving the whole problem numerically first. This is a salutary lesson for an applied mathematician.

For the alternative boundary condition (2.13), the problem can also be solved analytically for small and large Pe (Magar *et al.*, 2003). With pure diffusion, the spherically symmetric solution of (2.14) leads

$$\beta = 5 \quad (Pe = 10, 100)$$

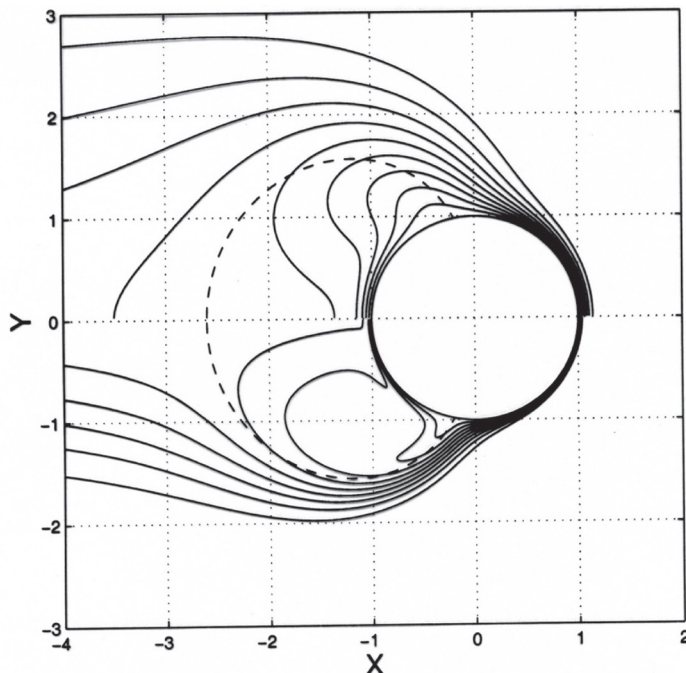


FIG. 7. Concentration contours for $\beta = 5$. The upper half is for $Pe = 10$, the lower half for $Pe = 100$. The step between contours is 0.1. From Magar *et al.* (2003).

to an expression for the nutrient uptake of the form

$$Q'_0 = 4\pi a D C_\infty \lambda, \quad (2.17)$$

where λ is a positive function of $\kappa, D_C/D$ and γ/D . At large Pe , for which the external boundary-layer thickness is $O(Pe^{-1/2})$, the rate-limiting step in mass transfer is consumption within the ‘cell’, not diffusion to it. To satisfy the boundary condition the external concentration gradient must remain $O(1)$, so the change in concentration across the boundary layer will be small, and the internal concentration distribution will still be approximately spherically symmetric. Then the Sherwood number, Sh' , equal to the uptake rate divided by Q'_0 , will be given to leading order by

$$Sh' = \gamma/D\lambda, \quad (2.18)$$

of $O(1)$ and independent of the flow. This quantity may be much greater than 1, but much less than the large- Pe value from the standard boundary condition. This is another salutary reminder, that we need to be certain of the relevant concentration boundary conditions when applying mass transfer theory to biological systems.

Michelin & Lauga (2011) have also solved the advection–diffusion equation (2.12) numerically, with the standard boundary condition, for a general steady squirm. Their main motive was again optimization: which squirming mode gives the largest nutrient uptake for a given expenditure (dissipation) of energy? The remarkable answer is that the optimum for nutrient uptake is very close to the neutral swimmer, already seen to be optimal for swimming. The result is not precise, nor a theorem, but Michelin & Lauga (2011) showed that $|B_n/B_1| << 1$ (see (2.3)) for $n > 1$ and all values of Pe . Another very interesting application of the steady spherical squirm model by these authors (Michelin *et al.*, 2013) is to synthetic particles with chemically active surfaces, for which the flow and the concentration distribution of reaction products are mutually coupled. A tangential gradient in the concentration leads to a tangential, phoretic, force being applied to the fluid next to the surface, and hence to a tangential slip velocity (Golestanian *et al.*, 2005). The contribution of Michelin *et al.* (2013) was to discover analytically that, even with a uniform distribution of reaction sites on the spherical surface, symmetry is broken when the Péclet number exceeds the critical value of 4, and the sphere then moves spontaneously in a process of autophoresis.

Although this subsection concerns mass transfer to or from steady squirmers, we may note that the corresponding problem for unsteady squirmers has been investigated by Magar & Pedley (2005) and by Michelin & Lauga (2013), in both cases for spheres with tangential surface velocities only. The former authors considered small amplitude ϵ oscillations in which the displacements of material elements on the surface were oscillatory functions of time with zero mean. The main interest in the analysis is that, for large Pe , the mean concentration distribution, leading to a non-zero mean nutrient uptake rate (necessarily of $O(\epsilon^2)$), satisfies a *steady* advection–diffusion equation in which, however, the advecting velocity field is not the same as the actual mean velocity field driven by the oscillatory squirming. Michelin & Lauga (2013) were again concerned with optimisation of both the flow and the nutrient uptake; their analysis was not confined to small-amplitude oscillations. Again they found that the squirming surface velocity optimal for mean nutrient uptake was the same as that for optimal swimming (i.e. maximum mean velocity for given energy dissipation) at all values of Pe . Surface displacements corresponding to the computed optimal swimming mode bore some resemblance to a metachronal wave.

3. Steady squirmers: hydrodynamic interactions and collective behaviour

One of the motives for studying micro-organisms is to be able to understand the behaviour of populations of them in lakes and oceans, for example, or in bioreactors. Therefore, suspensions of swimming cells have been studied in the laboratory, and a range of fascinating phenomena has been observed. For example, bioconvection patterns have been documented in suspensions of upswimming, denser-than-water, algae or bacteria, in finite-depth chambers, which generate gravitational instabilities (Wager, 1911; Platt, 1961; Kessler, 1985, 1986; Kessler *et al.*, 1994; Bees & Hill, 1997). These instabilities have been analysed for dilute suspensions by means of continuum models in which the cells interact with their environment through the cells' negative buoyancy, and through gravitational and viscous torques, but the swimmers do not interact directly with each other, hydrodynamically or otherwise (e.g. Childress *et al.*, 1975; Pedley & Kessler, 1992; Hillesdon & Pedley, 1996; Metcalfe & Pedley, 1998, 2001; Hill & Pedley, 2005; Bees & Hill, 1998, 1999; Pedley, 2010b). Non-gravitational instabilities have also been discovered in suspensions of bacteria (though not algae), driven by the stresses applied to the fluid by the swimmers themselves (Simha & Ramaswamy, 2002; Saintillan & Shelley, 2008; Ezhilan *et al.*, 2013). However, some of the most interesting observations have been made in concentrated suspensions of bacteria, with volume fractions around 30%, in which large-scale, random, time-dependent and coherent structures are observed—sometimes referred to as ‘bacterial turbulence’, although the Reynolds number of these

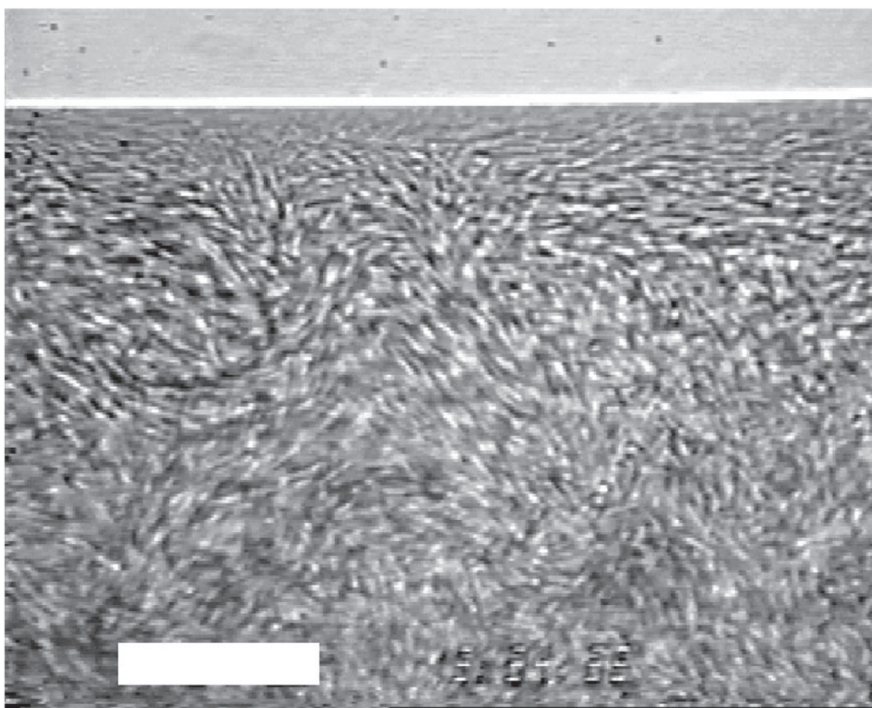


FIG. 8. Coherent structures of swimming bacteria in a sessile drop, viewed from below through the bottom of a petri dish. Gravity is perpendicular to the plane of the picture, and the horizontal white line near the top is the air-water-plastic contact line. Frame rate: 1/30 s; scale bar 35 μm . From Dombrowski *et al.* (2004).

structures is small (Dombrowski *et al.*, 2004) (Fig. 8). In these experiments there must be steric and hydrodynamic cell-cell interactions, as well (possibly) as chemical signalling.

3.1. Hydrodynamic interaction of two or more squirmers

The observations of Dombrowski *et al.* (2004) have been the incentive for investigating the hydrodynamics of cell-cell interactions, to see if they alone can explain coherent structures like those observed. In the same way as Batchelor & Green (1972a) began the analysis of non-dilute suspensions of passive particles by considering all possible pairwise interactions of two rigid spheres (Batchelor & Green, 1972b), so we began the study of suspensions of active particles by considering pairs of identical steady spherical squirmers (Ishikawa *et al.*, 2006). [Several of the following paragraphs are taken directly from Pedley (2010a).]

The hydrodynamic interaction of two squirmers (i.e. the force and torque exerted by one on the other) can be calculated analytically when they are sufficiently far apart ($r > 4a$, where r is the distance between the centres), using far-field expansions of the solutions of the Stokes equations, and when they are extremely close together ($r - 2a < 0.1a$), using lubrication theory. In between, the interaction is computed using the boundary element method. A database has been constructed of the effective force, torque and stresslet exerted by one squirmer on another for the whole range of relative positions and orientations, and trajectories of pairs of interacting cells can be traced. The most interesting trajectories

are two-dimensional ones, i.e. when the initial orientations of the two cells and the vector separating their two centres are coplanar. When the cells approach close to each other, very large rotations are predicted, with the consequence that the scattering angles, by which the trajectories are deflected by the ‘collisions’, are also very large—well over 90° in some cases. In other cases, bound pairs are formed. The results for three-dimensional trajectories are less dramatic, but the conclusion is that near-field interactions are responsible for significant scattering of cell trajectories and these effects would be missed if we treated the cells as oriented point particles, interacting only through the far field.

It should be remembered that these results were obtained for pairs of squirmers with prescribed surface velocities, so when they come very close together the viscous shear stress at the surface within the narrow gap will in general be very large, proportional to $\mu U/\epsilon a$ in a region of lateral extent $\epsilon^{1/2}a$, where ϵa is a scale for the gap width (Ishikawa *et al.*, 2006). For biological organisms, driven by beating cilia or flagella, the prescribed-shear-stress boundary condition (2.9) would probably be more appropriate, and one would expect the near-field effect to be different, though still important.

The next step was to use the database of pairwise interactions in simulations of a suspension of many swimming cells (Ishikawa & Pedley, 2007a). The initial positions and orientations of the squirmers were selected randomly but their trajectories were computed deterministically. An effectively infinite domain is achieved by using triply periodic boundary conditions in a cubic box of side L . Most of the results of Ishikawa & Pedley (2007a) were obtained from calculations with $N = 64$ cells; the volume fraction c was chosen in the range 0.025–0.1, since any higher value would invalidate the assumption that only pairwise interactions are significant. Later computations, using the more sophisticated Stokesian Dynamics method (Ishikawa & Pedley, 2008; Ishikawa *et al.*, 2008), were able to investigate a larger number of cells ($N = 216$) at higher values of c (up to 0.5). Visual inspection of movies of the whole collection of squirmers reveals little in the fully 3D case, because not all cells are visible at the same time. However, in two dimensions (for which c is the areal fraction) it can be clearly seen that jostling clusters or aggregates tend to form after a long enough time, with wide empty spaces between them. For $c \leq 0.1$, the length-scale of the clusters is well below the (periodic) system length-scale so that clustering is unlikely to be a computational artefact. For $c = 0.1$ and $\beta = \pm 5$, clusters tend to have a length-scale of around six cell diameters, and there is little correlation between the orientations of the cells in a cluster, which changes shape and membership in a chaotic manner. However, for $\beta = \pm 1$ there is a much stronger correlation, and a cluster can be regarded as a ‘phalanx’ of advancing cells for a considerable time (cf Cisneros *et al.*, 2007).

Very similar results were obtained by Zöttl & Stark (2014) who analysed the full hydrodynamics using the method of ‘multiparticle collision dynamics’, and considered a population of squirmers in quasi-two-dimensional confinement, i.e. swimming three-dimensionally but in a planar channel between no-slip walls whose spacing was 1.3 sphere diameters. They found small-scale clustering for the smallest c ($= 0.41$), with a tendency to larger clusters (in the form of hexagonal crystals) at larger c . The results depended strongly on β : at $c = 0.5$ there was almost complete phase separation for $\beta = 0$ and larger clusters for $\beta > 0$ (pullers) than for $\beta < 0$ (pushers); for $c \geq 0.64$ the cluster sizes decreased as $|\beta|$ increased, though for $c = 0.83$ phase separation was again almost complete.

The two-dimensional results receive qualitative support from the experiments of Thutupalli *et al.* (2011), using synthetic squirmers in a monolayer bounded by two solid, hydrophobic, plane boundaries. Their ‘squirmers’ were surfactant-covered droplets of an aqueous solution, suspended in oil, their motion being driven by Marangoni stresses; the effective value of β was close to zero (neutral squirmers), and the areal fraction c was either 0.46 or 0.78. Rather long-lived clusters of various sizes were formed, with high orientational correlation between close neighbours.

A somewhat different conclusion was reached by Matas-Navarro *et al.* (2014) from simulations of a fully-two-dimensional system of squirming discs in a thin, planar, viscous film between two semi-infinite fluids of much smaller viscosity. Previous simulations at high areal fraction, which included Brownian motion but ignored hydrodynamic interactions, clearly showed ‘motility induced phase separation’ (i.e. the formation of large clusters), but when hydrodynamic interactions were included this was almost totally suppressed, for all values of β and c . The suppression was attributed to the large changes of orientation caused by the frequent hydrodynamic interactions, which become more marked as the areal fraction is increased. However, why the results are so different from those of Ishikawa & Pedley (2008) or of Zöttl & Stark (2014) is unclear.

In three dimensions, in addition to the work of Ishikawa *et al.* (2008), simulations have been conducted on suspensions of steady squirmers by Evans *et al.* (2011), Alarcon & Pagonabarraga (2013) and Delmotte *et al.* (2015). The latter two groups used different computational methods and were able to investigate a very much larger number of squirmers, N , than Ishikawa *et al.* (2008) or Evans *et al.* (2011): Alarcon & Pagonabarraga (2013) used the Lattice Boltzmann method and simulated the motion of 2000 squirmers, while Delmotte *et al.* (2015) used the force-coupling method, developed for passive particles by Maxey & Patel (2001) and Lomholt & Maxey (2003), and made simulations involving over 37,000 particles. All these authors calculated both the radial distribution function $g(r)$ and an orientational (or polar) order parameter $P(t)$. Here $c_0 g(r) 4\pi r^2 dr$ is the average number of spheres whose centres lie at a distance between r and $r + dr$ from the centre of a particular sphere, computed in order to quantify the development of spatial order (clustering), and

$$P(t) = \frac{1}{N} \sum_{i=1}^N \mathbf{e}_i(t) , \quad (3.1)$$

where \mathbf{e}_i is the unit vector in the swimming direction of the i th squirmer (P was called $|\mathbf{e}_{\text{mean}}|$ by Ishikawa *et al.*, 2008). $P(t)$ was computed in order to examine to what extent the squirmers’ swimming is aligned. The steady-state ($t \rightarrow \infty$) radial distribution function, $g(r)$, shows a high peak close to contact, especially for pullers, and a secondary peak for $r/a - 2 \approx 0.25$, again for pullers, which reflects the already noted tendency to aggregation (Fig. 9, from Alarcon & Pagonabarraga, 2013). In all simulations $P(t)$ tends to a constant mean value, P_∞ , plus fluctuations, at large times. Both Evans *et al.* (2011) and Alarcon & Pagonabarraga (2013) agree that P_∞ does not depend significantly on the number density of squirmers (or, equivalently, on the box size L for a given number N of squirmers), but shows a significant dependence on squirming mode, β . This can be seen in Fig. 10, part (a) from Evans *et al.* (2011) and part (b) from Alarcon & Pagonabarraga (2013). Neutral squirmers ($\beta = 0$) show almost complete alignment, which drops off only slowly for $\beta > 0$ (pullers), while all but the weakest pushers ($\beta < 0$) show no alignment at all. Ishikawa *et al.* (2008) obtained the same result: strong alignment for $\beta = +1$ and very little alignment for $\beta = -1$, for both $c = 0.1$ and $c = 0.4$. However, the mechanism for the alignment, or ‘co-operative behaviour’, when it occurs, remains obscure although it must be hydrodynamic in origin. It deserves further study.

It should be remembered that the above results are for spherical squirmers only, not for elongated cells such as bacteria, for which geometric as well as hydrodynamic arguments for alignment between neighbours are compelling (Cisneros *et al.*, 2007; Aranson *et al.*, 2007; Saintillan & Shelley, 2012; Ezhilan *et al.*, 2013).

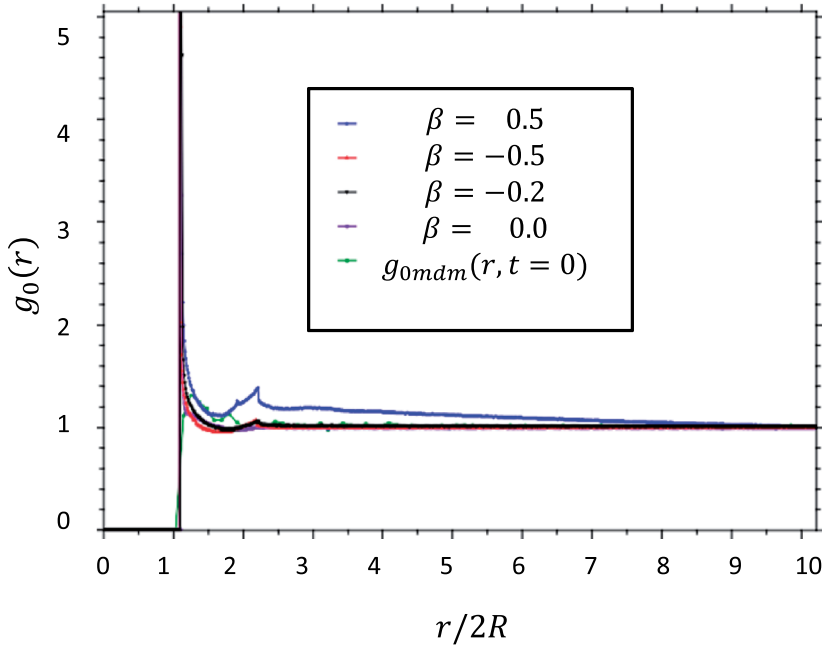


FIG. 9. Radial distribution function, $g_0(r)$, for puller ($\beta = 1/2$), pusher ($\beta = -1/2$ and $-1/5$), and neutral ($\beta = 0$) squirmer suspensions at $t/t_0 = 870$ time steps. $g_{0\text{mdm}}(r, t = 0)$ represents the initial configuration. From Alarcon & Pagonabarraga (2013).

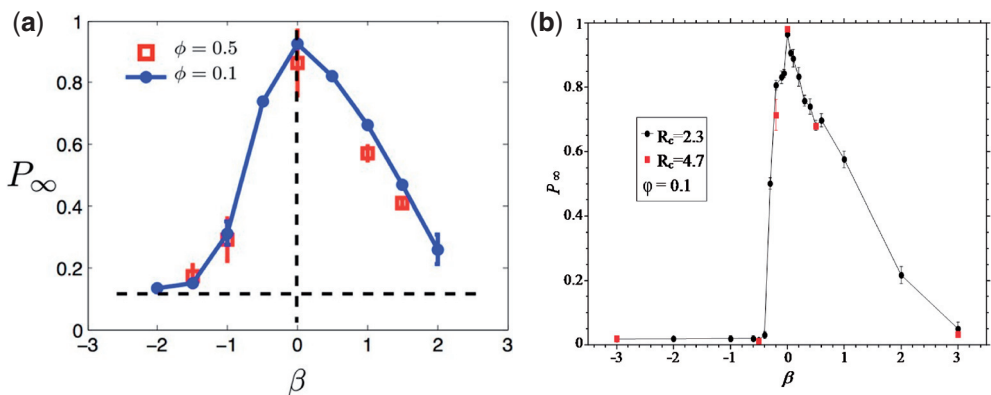


FIG. 10. The computed large time value, P_∞ , of the orientational order parameter at various values of β . (a) For $\phi = 0.1$ and 0.5 , where $\phi \equiv c$, from Evans *et al.* (2011); (b) for $\phi = 0.1$ and two different squirmer sizes, R_c , measured in terms of lattice spacing, from Alarcon & Pagonabarraga (2013).

3.2. Diffusive behaviour

A long-term goal of this research is to move from particle-based simulations of interacting cells to continuum models of concentrated suspensions. One important question is whether the random motion of cells subject to frequent ‘collisions’ with each other can be represented as a diffusive process with

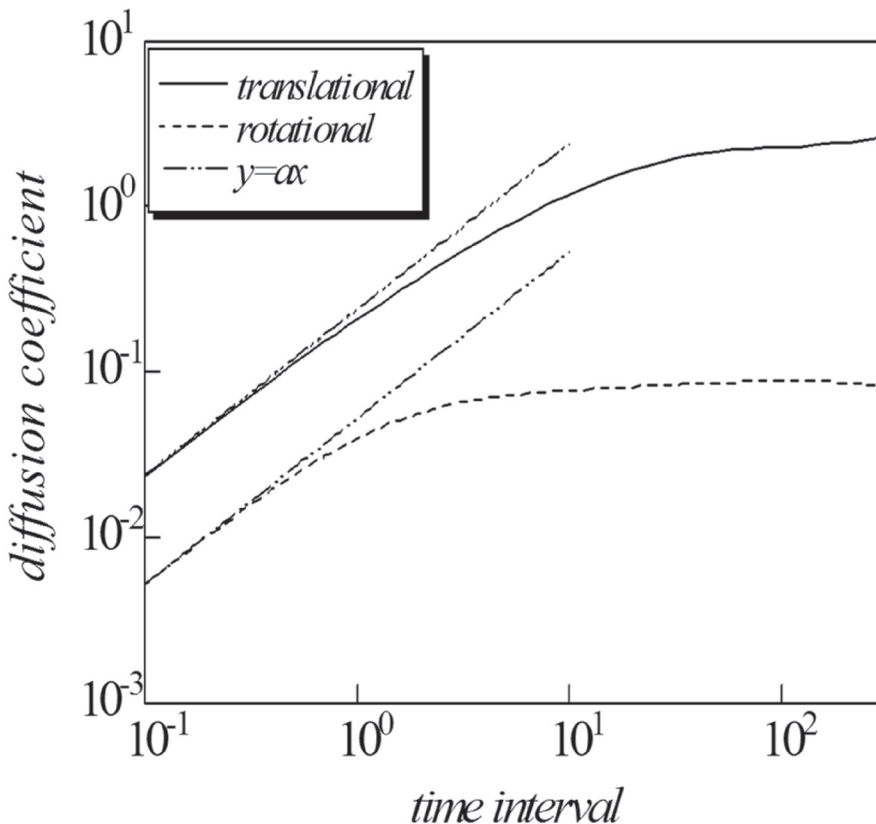


FIG. 11. Translational and rotational dispersion coefficients for squirmers in suspension, over the time interval Δt ($\beta = 5$ and $c = 0.1$). From Ishikawa & Pedley (2007a).

tensor or scalar translational and rotational diffusivities. This was investigated by Ishikawa & Pedley (2007a), who used their simulations to compute the mean-square linear and angular displacements of the squirmers as functions of time t . The effective translational dispersion (e.g.) may be defined as

$$\mathbf{D}_{\text{eff}}^T = \frac{\langle [\mathbf{r}(t) - \mathbf{r}(0)][\mathbf{r}(t) - \mathbf{r}(0)] \rangle}{2t}, \quad (3.2)$$

and similarly for rotational dispersion, $\mathbf{D}_{\text{eff}}^R$. If these quantities tend to constants as t tends to infinity, then the system does behave diffusively and these become the diffusivity tensors.

Assuming that the suspension behaves isotropically, we compute scalar quantities equal to one-third of the trace of $\mathbf{D}_{\text{eff}}^T$ and $\mathbf{D}_{\text{eff}}^R$, and these are plotted against time (for one case, $\beta = 5$ and $c = 0.1$) in Fig. 11. It can be seen that the quantities tend to constants after a long enough time (dimensionless time greater than about 20, where one time unit is the time it takes for a squirmer to swim a distance equal to its radius), so the system is diffusive, despite all the trajectories being deterministic (the initial conditions were random). However, if phenomena of interest take place on a shorter time scale, it would not be valid to represent cell spreading by a diffusivity.

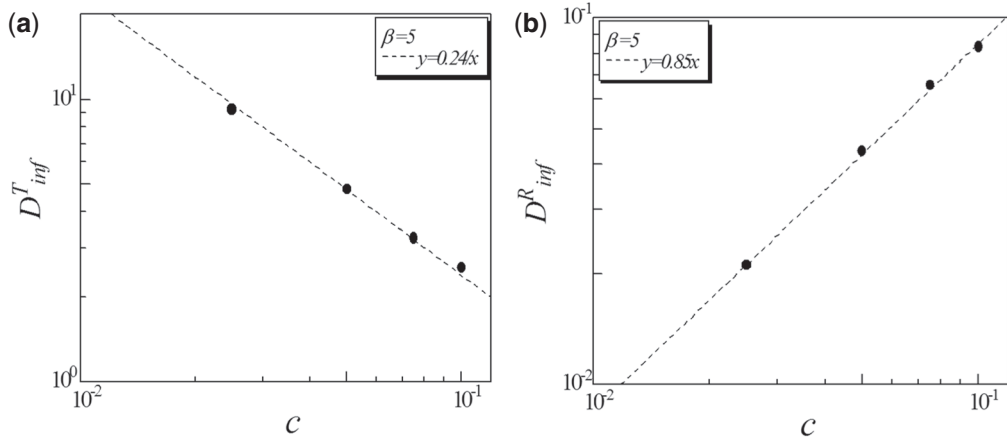


FIG. 12. Large time values of the effective diffusivities (a) translational, (b) rotational, as functions of c ($\beta = 5$). From Ishikawa & Pedley (2007a).

A simple scaling argument can be used to predict the dependence on the volume fraction of the large-time effective diffusivities and the time-scales for $\mathbf{D}_{\text{eff}}^{T,R}$ to become constant. The trajectory of a squirmmer, at least in a semi-dilute suspension (pairwise interactions dominant) considered by Ishikawa & Pedley (2007a), is a series of more-or-less straight runs interspersed by near-field collisions. Then the time scale for the collisions to dominate the cells' translation will be proportional to the mean time between collisions, t_{run} , and hence to $1/c$, while the time-scale for rotational randomisation will be proportional to the duration of a collision, t_{col} , and so independent of c . These predictions were borne out in the simulations (Ishikawa & Pedley, 2007a). Moreover, the translational diffusivity D^T should be proportional to $U^2 t_{\text{run}}$, and hence to $1/c$, while D^R should be proportional to $\langle \Delta \alpha^2 \rangle / t_{\text{run}}$, where $\langle \Delta \alpha^2 \rangle$ is the mean square angular displacement during a single collision, so $D^R \propto c$. These predictions are also borne out for simulations with $\beta = 5$ (Fig. 12).

3.3. Non-uniform suspensions

To be able to treat the random behaviour of interacting cells or squirmers as a diffusive process is a highly desirable assumption in the continuum modelling of suspensions in which the volume concentration of cells, c , varies with position, as in bioconvection (Pedley & Kessler, 1992; Pedley, 2010b; Saintillan & Shelley, 2008; Koch & Subramanian, 2011). However, it is likely to be valid only when the length scale over which the concentration varies is large compared with the length scales applicable to an individual cell's motion, in particular its mean free path,

$$\ell_{\text{mfp}} = U t_{\text{run}} \approx \frac{4a}{3c_0}, \quad (3.3)$$

where c_0 is the mean cell concentration (Ishikawa & Pedley, 2007a), but there has been very little study of situations in which that is not the case. Ishikawa & Pedley (2014) began such a study by conducting simulations, using their modified Stokesian Dynamics method, for a suspension in which the initial

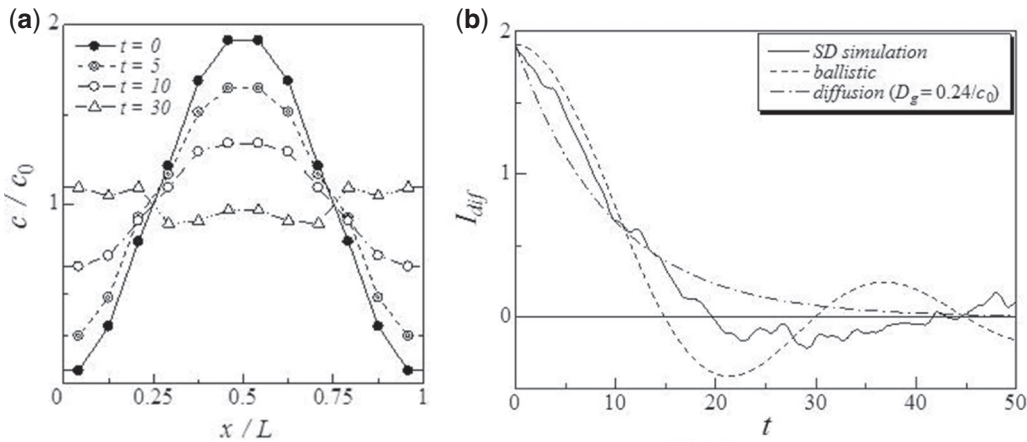


FIG. 13. (a) Change of dimensionless concentration distribution over the time $t = 0 - 30$ ($c_0 = 0.1, \beta = 1, L = 30$): black circles $t = 0$, grey circles $t = 5$, open circles $t = 10$, open triangles $t = 20$, open triangles $t = 30$. (b) I_{diff} as function of time for $c_0 = 0.1, \beta = 5, L = 30$; solid line: Stokesian Dynamics simulation, dash-dot line: pure diffusion, dashed line: assuming ballistic trajectories. From Ishikawa & Pedley (2014).

macroscopic concentration varied sinusoidally along one coordinate direction, x , according to

$$c(x) = c_0 \left[1 - \cos \left(\frac{2\pi x}{L} \right) \right], \quad (3.4)$$

where L is the wavelength. There is no macroscopic concentration variation in the perpendicular y and z directions. The initial positions of individual squirmers are randomly distributed in such a way as to satisfy (3.4); the initial orientations of the squirmers are also random and distributed isotropically. A suspension of infinite extent is represented by periodic boundary conditions in all three directions. A unit computational domain is a rectangle with the side length L in the x direction. The side lengths in the y and z directions, L_y and L_z , are given so as to satisfy the suspension average volume fraction c_0 with 900 squirmers, i.e. $L_y = L_z = \sqrt{1200\pi/c_0 L}$. All equations are non-dimensionalized using the radius a of a squirmer, the swimming speed of a solitary cell U_0 and the fluid viscosity μ .

The range of parameters used in the study were as follows: volume fraction $0.05 \leq c_0 \leq 0.15$; swimming mode $-5 \leq \beta \leq 5$; system size $22.5 \leq L \leq 60$. By assuming the mean free path of squirmers to be as given by (3.3), the system size may be rewritten as $1.7\ell_{\text{mfp}} \leq L \leq 4.5\ell_{\text{mfp}}$ when $c_0 = 0.1$. These values are employed in order to investigate the system when the local equilibrium hypothesis breaks down, while keeping enough particles in each x section to calculate ensemble averages.

A sample of the results is given in Fig. 13. Figure 13(a) shows how the concentration distribution varies with time from $t = 0$ to $t = 30$: the distribution is initially sinusoidal, but the amplitude of the concentration difference between $x = L/2$ and $x = 0$ decays between $t = 0$ and $t = 10$. At $t = 20$, however, the concentration at $x = 0$ becomes considerably higher than that at $x = L/2$, an overshoot which is inconsistent with pure diffusion.

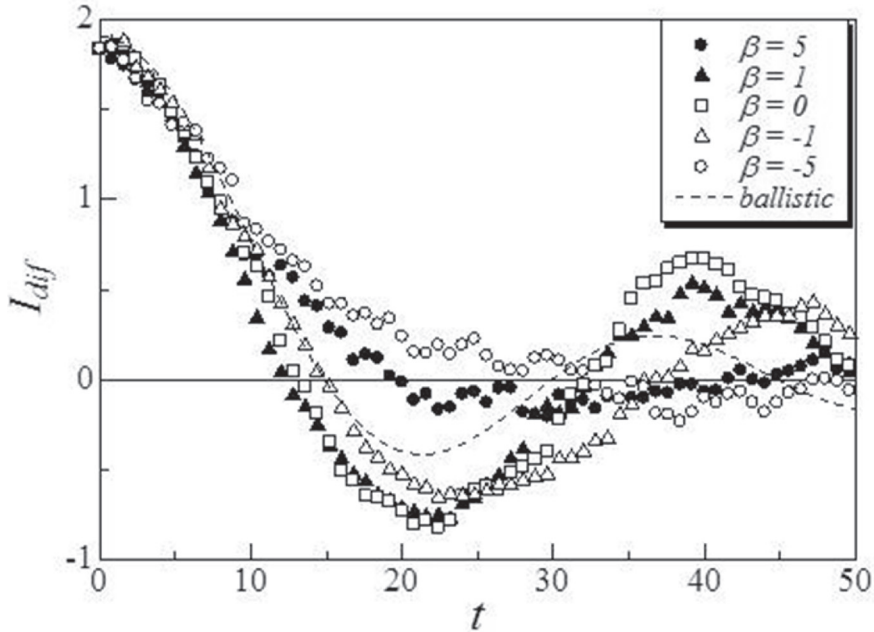


FIG. 14. I_{diff} as function of time for various values of β ; dashed line: ballistic trajectories. From Ishikawa & Pedley (2014).

The decay process of the concentration variation can be simply represented by an index I_{dif} defined by:

$$I_{\text{dif}} = \frac{1}{2\delta c_0} \left[\int_{\frac{L}{2}-\delta}^{\frac{L}{2}+\delta} c \, dx - \int_0^\delta c \, dx - \int_{L-\delta}^L c \, dx \right]. \quad (3.5)$$

This indicates the dimension-free concentration difference between $x = L/2$ and $x = 0$ (or $x = L$), where the concentration is initially maximum and minimum, respectively. As the concentration distribution eventually becomes homogeneous, I_{dif} converges to zero. If the spreading process were diffusive, I_{dif} would never become negative; if the spreading were ballistic, on the other hand, I_{dif} would go negative (see Fig. 13(b)). Thus, I_{dif} is a convenient indicator of whether the spreading process is more diffusive or more ballistic. The parameter δ controls the width of the averaging region, though varying it does not change the results qualitatively. In order to have enough particles in each region while keeping a clear distinction between regions, δ was taken equal to $L/12$ throughout.

The effect of β on the time change of I_{dif} is shown in Fig. 14 ($c_0 = 0.1$ and $L = 30$), β being the ratio of second mode squirming to first mode squirming. The result for purely ballistic motion can be derived as:

$$I_{\text{dif}}(t) = \frac{6}{\pi} \frac{L}{2\pi U_0 t} \sin \left(\frac{2\pi U_0 t}{L} \right), \quad (3.6)$$

which is also plotted for comparison. We see that the effect of β is very large. A surprising result is that, when $|\beta|$ is small, the curve of I_{dif} oscillates more than the analytical result for ballistic swimming. The case of the neutral squirm ($\beta = 0$) shows the most extreme oscillation in I_{dif} , while the difference between pullers and pushers is here less marked, though pullers ($\beta > 0$) do show greater oscillation than pushers. The fact that the squirm concentration for smaller values of β oscillates more even than if their motion were purely ballistic is consistent with the fact that the hydrodynamic interactions cause at least some of the squirms to align their motion with that of their neighbours: to cooperate, as it were. This is consistent with the findings of Evans *et al.* (2011), Alarcon & Pagonabarraga (2013) and Delmotte *et al.* (2015) that have already been discussed.

3.4. Suspensions of bottom-heavy squirms

All the above studies on the collective behaviour of squirms in suspension are concerned with circumstances in which the ambient fluid is at rest, apart from the flow induced by the squirms themselves, and the squirms do not experience any external, e.g. gravitational, force or torque. Most micro-organisms are slightly denser than water, and sediment if not swimming. However, their sedimentation speed is typically very much less than their swimming speed, so the effect of sedimentation on the hydrodynamic interaction between and collective behaviour of squirms has not been studied. On the other hand, some motile algal species are known to be bottom-heavy, with centre of mass behind the centre of buoyancy, as are *Volvox* colonies. The resulting gravitational torque, when the cells' axes are not vertical, has a big effect on their orientation and hence on their swimming direction. This in turn determines their effect on the fluid flow, leading to a so-called 'gyrotactic' mechanism for bioconvective instability, in addition to that which results from the unstable density stratification generated in a finite-depth fluid layer by the cells' upswimming (Pedley & Kessler, 1992).

Some simulations of suspensions of bottom-heavy steady squirms have been conducted by Ishikawa & Pedley (2007a,b), Ishikawa *et al.* (2008) and Ishikawa & Pedley (2008). The parameter indicating the importance of bottom-heaviness is

$$G_{bh} = \frac{2\pi\rho gah}{\mu B_1}, \quad (3.7)$$

where h is the distance from the centre of the sphere to the centre of mass. Thus G_{bh} is the ratio of the time scale for the sphere to swim one radius, a/B_1 , to the time for gravitational reorientation after the axis is tilted by an $O(1)$ angle from the vertical. If we take $h \approx 0.1a$ and use measured values of a and $U_0 (= \frac{2}{3}B_1)$ (Kessler, 1986; Drescher *et al.*, 2009), we see that $G_{bh} \approx 1.5$ for *Chlamydomonas* and may be as large as 500 or greater for *Volvox*. The initial condition for each simulation of up to 216 squirms was again isotropically random orientation and homogeneously random position. Overlapping of two spheres was prevented by a strong, short-range repulsive force which is switched on when the distance of closest approach becomes extremely small; otherwise the near field hydrodynamics is computed exactly, as for non-bottom-heavy squirms. Neither in two dimensions (a monolayer of squirms in an infinite fluid) nor in three has the relevant parameter space, of G_{bh} , β and c_0 been explored very fully. Clearly, however, the squirms swim upwards, on average, for every positive value of G_{bh} .

In two dimensions, the tendency to cluster into clumps for $G_{bh} = 0$ is replaced at large enough G_{bh} by a tendency to form stable structures that span the whole horizontal (periodic) domain. These take the form of chevron-like lines for $G_{bh} = 100, \beta = 1, c_0 = 0.1$ (Fig. 15(a)) or relatively deep structures resembling liquid crystals for $G_{bh} = 100, \beta = 1, c_0 = 0.5$ (Fig. 15(b)). These figures are

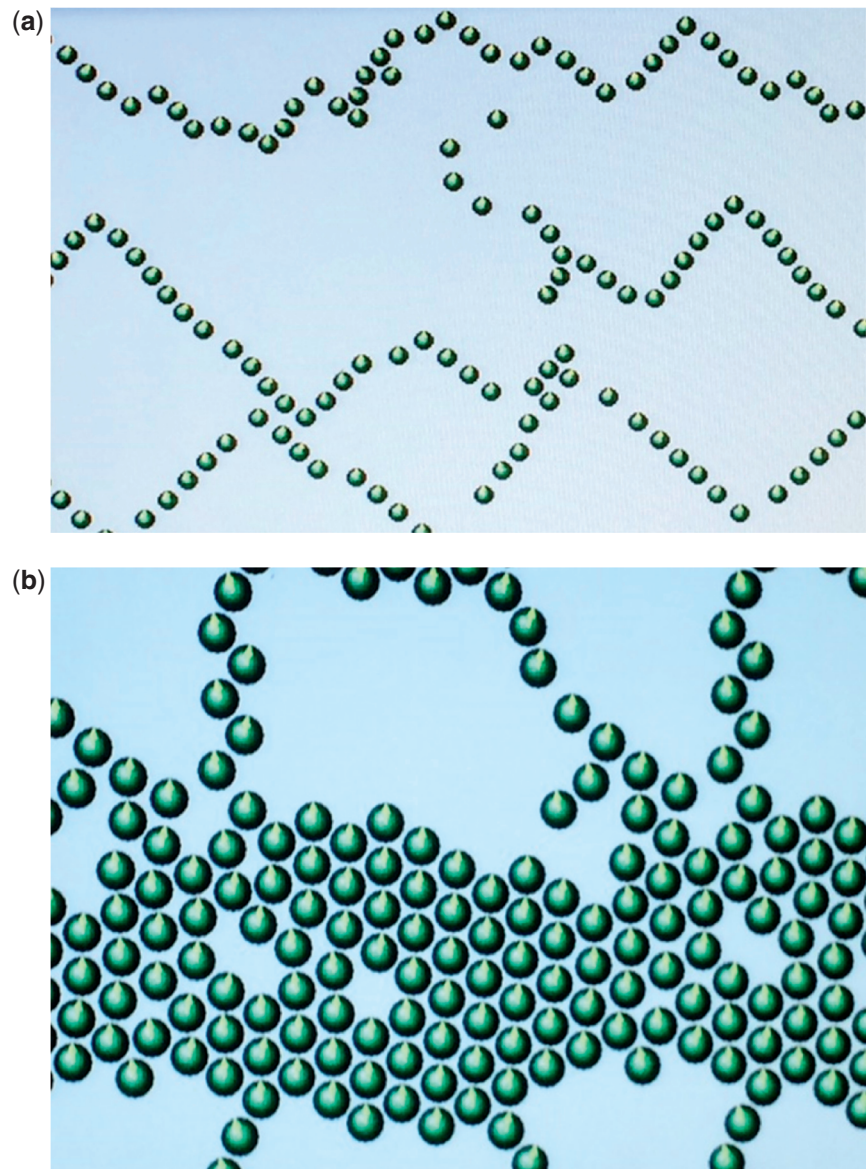


FIG. 15. Stills from simulations of squirmer suspensions in a monolayer (i.e. with two-dimensional trajectories). (a) $c = 0.1, \beta = 1, G_{bh} = 100$; (b) $c = 0.5, \beta = 1, G_{bh} = 100$. Computed using the simulation of Ishikawa & Pedley (2008); figures kindly supplied by Prof. T. Ishikawa.

stills from movies, in which the squirmers are seen to jiggle around in response to their hydrodynamic interactions.

The stability of a homogeneous, planar, crystalline array of squirmers at large c_0 (so that the undisturbed narrowest gap between spheres was $\epsilon_0 a$, $\epsilon_0 = 2 \times 10^{-3}$) has been investigated semi-analytically by Brumley (2013). He used lubrication theory to describe the fluid dynamics in the narrow spaces

between every pair of neighbouring squirmers, whose positions and orientations were given small, in-plane perturbations. The calculation showed that the array is always unstable if there is no short-range repulsive force. When there is a repulsive force, as in the computations of Ishikawa & Pedley (2008), the array is stable if G_{bh} exceeds a critical value, depending on the squirming parameter β : the critical value is approximately 45 when $\beta = 1$. When out-of-plane perturbations were allowed, the array was of course unstable. However, when the array was confined between two vertical, rigid, no-slip, plane boundaries, with the unperturbed narrowest gap between a sphere and one plane equal to $\epsilon_1 a$ ($\epsilon_1 = 5 \times 10^{-3}$), but three-dimensional perturbations were allowed, the results were essentially the same as for the unconfined monolayer, in that the array is unstable for $G_{bh} = 0, \beta = 1$ and stable for $G_{bh} = 50, \beta = 1$ (no further values of G_{bh} or β were considered by Brumley, 2013). This result is both interesting, because the far-field behaviour in a confined monolayer is quite different from that in an unconfined one, and practically satisfying, because confining the monolayer in a narrow channel represents a potentially realistic experiment.

As for non-bottom-heavy squirmers, there is no readily visible clustering during fully three-dimensional simulations of bottom-heavy squirmers. However, one can again use the computations to investigate the diffusive properties of the suspension, in both two and three dimensions. Results are given by Ishikawa & Pedley (2007a). In calculating the effective dispersion, D_{eff}^T , from (3.2), one must measure the displacement $\mathbf{r}(t)$ in a frame of reference that translates vertically upwards with the average upswimming velocity, which decreases as c_0 is increased because of the increased frequency of near-field encounters. Unsurprisingly, the effective diffusivity tensor is no longer isotropic when G_{bh} is non-zero. The horizontal effective diffusivity tends to a constant at large times, as in Fig. 11, and the long-time value of $D_{\text{eff}}^{\text{horiz}}$ decreases as G_{bh} increases, as is expected because whatever the collisional perturbations, the orientation vector always tends towards the vertical. Less obviously, the vertical effective diffusivity also tends to a constant, relative to the moving frame, though its value is not the same as the horizontal one (Ishikawa & Pedley, 2007a). Qualitatively, these findings are not significantly affected by the values of β and c_0 .

3.5. Suspension rheology

A long-standing motive for studying the hydrodynamics of suspensions and emulsions has been the need to know their macroscopic rheological properties, both out of fundamental scientific interest and because of their widespread industrial applications (in the construction, oil, paper, chemical, food and other industries). When a suspension in a Newtonian liquid is subjected to a shear or straining flow whose length scale is much greater than the particle size or spacing, the flow can be approximated by a linear velocity gradient. If there were no particles present the deviatoric stress Σ would be

$$\Sigma = 2\mu_0 \mathbf{E}, \quad (3.8)$$

where \mathbf{E} is the strain-rate tensor and μ_0 is the viscosity of the suspending fluid. The presence of particles makes a difference, because a particle does not deform or rotate in the same way as the fluid would if the particle were not there, with the result that there is an additional contribution to the stress tensor. The leading order effect for a dilute suspension of identical rigid spheres, in which particles do not interact (small volume fraction c), was calculated by Einstein (1906), who showed that (3.8) is still valid as long as μ_0 is replaced by

$$\mu = \mu_0 \left(1 + \frac{5}{2}c\right). \quad (3.9)$$

Batchelor (1970) analysed the bulk stress in a suspension of non-spherical, force-free but not torque-free, particles. Batchelor & Green (1972a) and Batchelor (1977) were the first to incorporate the effects of pairwise particle interactions into the theory and, for spherical particles at small c , calculated the $O(c^2)$ correction to (3.9) ($\mu/\mu_0 = 1 + 5c/2 + 6.2c^2$). In Batchelor's theory, as in Einstein's, the distributions of spheres in different realisations of the suspension are supposed to be independent random distributions as a result of arbitrary initial conditions or Brownian motion. The theory has been the basis of many studies over the last 45 years. Ishikawa & Pedley (2007b) sought to extend the Batchelor analysis for suspensions of active spheres in the form of steady squirmers. The leading order rheological feature of an active suspension comes from the fact that, in general, every cell exerts a force-dipole, or stresslet, on the fluid, leading to a particle-stress tensor, $\Sigma^{(p)}$, that must be added to the hydrodynamic stress tensor. Here

$$\Sigma^{(p)} = cS \left(\langle \mathbf{e}\mathbf{e} \rangle - \frac{1}{3} \mathbf{I} \right), \quad (3.10)$$

where c is the volume fraction of particles, S is the stresslet strength of one particle ($= 4\pi\mu a^2 B_2$ from (2.3)), \mathbf{e} is the unit vector in the swimming direction of a particle, and the average is taken over \mathbf{e} -space, the unit sphere. Moreover, there are differences, due to swimming and hydrodynamic interactions, in both the $O(c)$ and the $O(c^2)$ terms in the expression for apparent suspension viscosity μ/μ_0 . However, for non-bottom-heavy squirmers Ishikawa & Pedley (2007b) showed that these differences are small: the $O(c)$ term in the apparent viscosity is reduced by less than 5% whatever the values of β ($|\beta| \leq 10$) or the squirming velocity relative to the applied shear $\dot{\gamma}$ (i.e. $Sq = 2B_1/3a\dot{\gamma}$). The $O(c^2)$ term is approximately the same as that resulting from Brownian motion (Batchelor & Green, 1972a).

The situation is different for bottom-heavy squirmers, however, because the spheres are now subjected to an external torque and the distribution of the squirmers' swimming directions is no longer isotropic, even in the absence of interaction. Instead it is determined by the gravity-viscous torque balance (as well as Brownian motion if that is significant). The effect on the apparent shear viscosity depends strongly on the orientation of the shear flow relative to gravity. When the flow is horizontal (in the x -direction) and the velocity gradient is vertical, the squirmers tend to swim across streamlines, carrying x -momentum with them, and the apparent viscosity is substantially increased—by a factor of more than 2 for $G_{bh} = 100$, $\beta = 5$, $Sq = 1$, $c = 0.1$. When the flow is vertical, on the other hand, the apparent viscosity is lower than that for inert spheres, and may even be lower than that of the suspending fluid if G_{bh} is large enough. In both cases there is also a substantial non-Newtonian effect, represented by the appearance of normal stress differences.

Thus, without bottom-heaviness, the effect of swimming on the rheology of a suspension of identical spheres is minor, but when the external gravitational torque is added, the effect depends strongly on the orientation of the simple shear flow relative to gravity. Moreover, no computations have been performed for squirmers in any other linear flow such as a pure straining motion. The situation for non-spherical swimmers is quite different, because even without an external torque, elongated particles in a simple shear flow (for example) tend to be aligned preferentially close to the flow direction, with a perturbation towards the direction of maximum extension in the flow (Hinch & Leal, 1972). In a pure straining motion, elongated particles align with the direction of maximum extension. In both cases, if the particles are pushers, they naturally generate an extensional flow, thereby reducing the effective bulk viscosity of the suspension, but have the opposite effect if they are pullers. In non-dilute suspensions, elongated pushers (such as bacteria) tend to align anyway, for geometric reasons, so the effect on vis-

cosity is enhanced. The theory for elongated active particles is given by Hatwalne *et al.* (2004), Haines *et al.* (2009) and Saintillan (2010); the predicted reduction in viscosity for pushers is consistent with experiments on bacterial suspensions by Sokolov & Aranson (2009, 2012). A corresponding increase in effective viscosity predicted for suspensions of pullers is also consistent with experiments on motile algae by Rafai *et al.* (2010). However, these effects, although extremely interesting, require that the cells' orientation distribution becomes markedly anisotropic in an imposed shear or straining flow, and cannot be investigated by modelling the cells as spherical squirmers.

The range of additional phenomena to which the steady spherical squirmer model has been applied continues to be extended in various ways: to swimming in a stratified fluid, with potential relevance to micro-organisms in lakes and oceans (Doostmohammadi *et al.*, 2012); to squirmers moving near a plane boundary (Ishimoto & Gaffney, 2013; Li & Ardekani, 2014) or in a confined geometry of similar width to the squirmer itself, such as a tube (Zhu *et al.*, 2013) or a planar channel (including nutrient uptake—Lambert *et al.*, 2013); to tracer particle dispersion in a suspension of swimmers (Lin *et al.*, 2011; Thiffeault & Childress, 2010; Pushkin *et al.*, 2013; Ishikawa *et al.*, 2010; Eckhardt & Zammert, 2012) for which there are well-known experimental data (Wu & Libchaber, 2000; Leptos *et al.*, 2009); and to time-dependent squirming (Michelin & Lauga, 2013; Wang & Ardekani, 2012; Giacché & Ishikawa, 2010). The remainder of this article will be concerned with only the last of these.

4. Unsteady squirmers

We now turn to unsteady squirmers, and in general permit both radial and tangential, time-dependent, surface velocities; i.e. the coefficients A_n , B_n in (2.3) are functions of time t , with a characteristic frequency σ . We still assume the flow to be governed by the Stokes equations, implying that both convective and local inertia are negligible; i.e. both the Reynolds number $Re = U_0 a / \nu$ and the frequency parameter $S = \sigma a^2 / \nu$ are small compared with unity. Here U_0 is a typical velocity of the squirmer envelope and, in application to the swimming of ciliates and *Volvox*, this comes about as a result of oscillations of material points on the surface, of amplitude ϵa ($\epsilon \ll 1$) and frequency σ , so $U_0 = \epsilon \sigma a$, and $Re = \epsilon S$; we take $Re \ll S \ll 1$. Thus the velocity field is again given by (2.1), in which U is the instantaneous speed of translation of the sphere. If the sphere is neutrally buoyant, it experiences no external force, so the Stokeslet term must still be zero, and

$$U = \frac{2}{3}B_1 - \frac{1}{3}A_1 \quad (4.1)$$

(Blake, 1971). In fact A_1 should be taken to be zero, because it corresponds to longitudinal translation of the centre of the sphere which is incorporated in U .

The ‘envelope model’ of Lighthill (1952) and Blake (1971) showed that, although the Stokes equations are linear, small-amplitude oscillations of material elements on the surface lead to a non-zero mean swimming speed at $O(\epsilon^2)$ because of geometric non-linearity. Let the Lagrangian co-ordinates (R, θ) of a material element whose mean location is (a, θ_0) be given by

$$R - a = a\epsilon \sum_{n=0}^{\infty} \alpha_n(t) P_n(\cos \theta_0) \quad (4.2a)$$

$$\theta - \theta_0 = \epsilon \sum_{n=1}^{\infty} \beta_n(t) V_n(\cos \theta_0). \quad (4.2b)$$

Then at the boundary the Eulerian velocity field is related to \dot{R} and $\dot{\theta}$ by

$$(\dot{R}, R\dot{\theta}) = [u_r(R, \theta), u_\theta(R, \theta)] \quad (4.3)$$

and

$$\mathbf{u}(R, \theta) = \mathbf{u}(a, \theta_0) + (R - a) \left. \frac{\partial \mathbf{u}}{\partial r} \right|_{a, \theta_0} + (\theta - \theta_0) \left. \frac{\partial \mathbf{u}}{\partial \theta} \right|_{a, \theta_0} + \dots \quad (4.4)$$

Thus, in the simplest example, in which α_n and A_n are zero (purely tangential motions on the spherical surface), one obtains:

$$U = \frac{2}{3}B_1 = \frac{2}{3}\epsilon a\dot{\beta}_1 + 4\epsilon^2 a \sum_{n=1}^{\infty} \frac{(n+2)\beta_n\dot{\beta}_{n+1} - n\dot{\beta}_n\beta_{n+1}}{(n+1)(2n+1)(2n+3)}. \quad (4.5)$$

In general the ϵ^2 -terms will have non-zero mean even though the β_n are oscillatory with zero mean; the mean swimming speed in this case, from (4.1), is $O(\epsilon^2)$ and equal to the average of the last term in (4.5) (Blake, 1971).

In a recent article, Pedley *et al.* (2016) have made two significant extensions to the Lighthill-Blake model, with α_n and A_n non-zero, in order to apply it to *Volvox*. The first was to incorporate azimuthal swirl into the model, to account for the facts that the flagella of *Volvox* all beat at an angle of 10°–20° to the local meridional plane and that the whole colony rotates about its axis of symmetry. The general solution of the azimuthal, ϕ -, component of the Stokes equations is

$$u_\phi(r, \theta_0) = \sum_{n=1}^{\infty} C_n \frac{a^{n+2}}{r^{n+1}} V_n(\cos \theta_0), \quad (4.6)$$

with $C_1 = 0$ because the free-swimming colony is torque-free. The ϕ -displacement of a material point on the rotating surface must be proportional to the θ -displacement, so

$$(\phi - \phi_0) \sin \theta_0 = \int \Omega dt \sin \theta_0 + \epsilon \sum_{n=1}^{\infty} \gamma_n(t) V_n(\cos \theta_0), \quad (4.7)$$

where ϕ_0 is fixed on the rotating sphere, and Ω is the instantaneous angular velocity of the sphere. Adding $u_\phi(R, \theta) = r \sin \theta \dot{\phi}$ into (4.3), and following a similar analysis to Blake's, eventually gives

$$\Omega = -\epsilon \dot{\gamma}_1 + \epsilon^2 \Omega^{(2)} \quad (4.8)$$

where

$$\begin{aligned} \Omega^{(2)} = & -\frac{4}{5}\beta_1\dot{\gamma}_2 + \sum_{n=2}^{\infty} \frac{3}{(2n+1)(2n+3)} [-(n+3)\alpha_n\dot{\gamma}_{n+1} + (n+2)\alpha_{n+1}\dot{\gamma}_n] \\ & + \sum_{n=2}^{\infty} \frac{6}{(2n+1)(2n+3)(n+1)} [-(n+3)\beta_n\dot{\gamma}_{n+1} + (n-1)\beta_{n+1}\dot{\gamma}_n]. \end{aligned} \quad (4.9)$$

Mention should also be made of the recent articles by [Pak & Lauga \(2014\)](#), by [Ghose & Adhikari \(2014\)](#) and by [Felderhof & Jones \(2016\)](#), who all set out the general flow field for a squirmer with not only swirl but also ϕ -dependence of the surface ($r = a$) velocities, but only [Felderhof & Jones \(2016\)](#) related the surface velocities to Lagrangian displacements of surface elements.

The second extension to the envelope model was to use real data for the surface displacements $\alpha_n, \beta_n, \gamma_n$. [Brumley et al. \(2012\)](#) used Micro Particle Image Velocimetry to measure the tangential (θ) and radial (r) fluid velocities just outside the layer of beating flagella on *Volvox carteri* colonies held at rest on a micro-pipette. They found clear evidence that the flagellar beating takes the form of a symplectic metachronal wave (symplectic means beating in the same direction as the power stroke of each flagellum, see Fig. 2), so that the displacement of a flagellar tip, assumed to be elliptical, is given by

$$R - a = a\epsilon \sin(k\theta_0 - \sigma t), \quad \theta - \theta_0 = \epsilon\delta \cos(k\theta_0 - \sigma t) \quad (4.10)$$

so, from (4.2),

$$\alpha_0(t) + \sum_{n=2}^{\infty} \alpha_n(t) P_n(\cos \theta_0) = \sin(k\theta_0 - \sigma t) \quad (4.11a)$$

$$\sum_{n=1}^{\infty} \beta_n(t) V_n(\cos \theta_0) = \delta \cos(k\theta_0 - \sigma t) \quad (4.11b)$$

and, by extension,

$$\sum_{n=1}^{\infty} \gamma_n(t) V_n(\cos \theta_0) = \tau \delta \cos(k\theta_0 - \sigma t). \quad (4.12)$$

Evaluating the $\alpha_n, \beta_n, \gamma_n$ from (4.10) and (4.11), and inserting them in equation (2.17) from [Pedley et al. \(2016\)](#) and (4.9) above gives

$$\begin{aligned} \bar{U} = & -2\epsilon^2 a\sigma \delta Z(1) \sin k\pi (12\delta - \frac{9}{k}) + \epsilon^2 a\sigma \sin k\pi \sum_{n=2}^{\infty} (-1)^n Z(n) \\ & \times [2\delta^2 n(n+1)^2(n+2) - 2k\delta(n+1)(2n^2 + 3n + 2) - k^2(2n^2 - 2n - 1)] \end{aligned} \quad (4.13)$$

and

$$\begin{aligned} \bar{\Omega} = & 36\epsilon^2 \sigma \tau \delta^2 Z(1) \sin k\pi \\ & + \frac{3}{2} \epsilon^2 \sigma \tau \delta \sin k\pi \sum_{n=2}^{\infty} (-1)^n Z(n)(n+1)(n+2)[(2n+3)k + 2\delta n(n+1)], \end{aligned} \quad (4.14)$$

where

$$Z(n) = \frac{1}{4((n+2)^2 - k^2)((n+1)^2 - k^2)(n^2 - k^2)}. \quad (4.15)$$

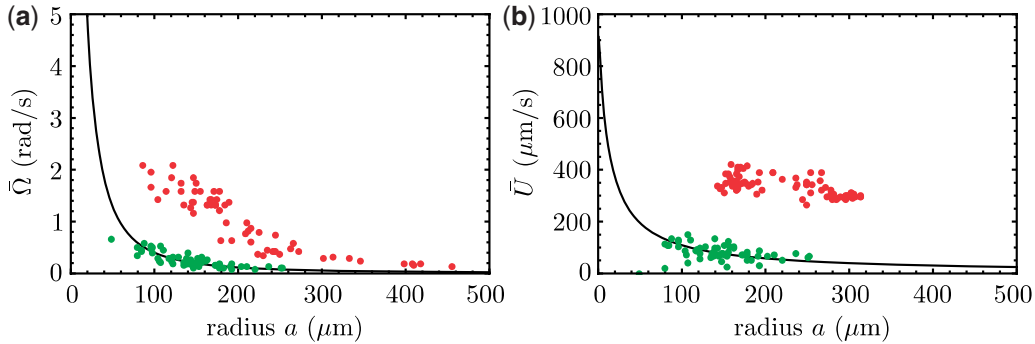


FIG. 16. Predicted and measured values of (a) mean angular velocity $\bar{\Omega}$ and (b) mean swimming speed \bar{U} , as functions of *Volvox* colony radius. Green dots are predictions of this model, red dots are measurements (on a different population of colonies) by Drescher *et al.* (2009). Solid line is the prediction from mean properties of the 60 colonies whose metachronal wave data have been used. Here the mean amplitude $\epsilon \approx 0.035$, equivalent to flagellar length $L = 20 \mu\text{m}$. From Pedley *et al.* (2016).

Brumley *et al.* (2012) evaluated the wave number k and frequency σ for each of 60 colonies of various radii. From their data one can also estimate an average value for the ratio of the major to the minor axis of the assumed elliptical orbit of a flagellar tip (δ). The amplitude parameter ϵ is taken to be one third of the flagellar length divided by the colony radius a ; the azimuthal offset angle is taken to be $\tan^{-1} \tau = 15^\circ$. The predicted values of \bar{U} and $\bar{\Omega}$ are then plotted as functions of a in Fig. 16. Also plotted are measurements of \bar{U} and $\bar{\Omega}$ made a few years ago on 60–80 colonies of the same species (also in the Cambridge laboratory set up by Professor Raymond Goldstein) by Drescher *et al.* (2009). In this case the plotted value of \bar{U} is the sum of the measured upswimming speed and the sedimentation speed of a non-swimming colony of the same radius, since the colonies are a little denser than water; the above theory assumes neutral buoyancy. We see that the trend with increasing radius agrees qualitatively with observation, but the predictions for both \bar{U} and $\bar{\Omega}$ are significantly below the measured values, despite the instantaneous velocities of material points on the envelope being somewhat overestimated. This is in part due to the fact that the envelope model is unlikely to be accurate for flagella that are spaced as widely as they are on *Volvox*, with a spacing of 10–20 μm , comparable to the flagellar length. (Agreement becomes excellent if one increases the amplitude parameter from 0.035 to 0.082, corresponding to a flagellar length of 50 μm instead of 20 μm .) However, the main source of the underestimate is attributed to the fact that the flow driven by the recovery stroke of a flagellum is slowed down more by the proximity of the no-slip substrate than is that driven by the power stroke, which is not accounted for in the model. A full computational fluid dynamic analysis of the beating flagella is clearly called for.

The effect of (local) inertia on an unsteady spherical squirmer with surface displacements that are tangential only ($\alpha_n = \gamma_n = 0$) has been analysed by Felderhof & Jones (1994) and by Wang & Ardekani (2012) for oscillatory functions $\beta_n(t)$ (see (4.2b)) with zero mean. The authors took the frequency parameter S to be $O(1)$, while the Reynolds number Re was still $\ll 1$, so the Navier–Stokes equations remained linear: they include the Basset force and added mass, but not convective inertia. Wang & Ardekani (2012) analytically calculated the swimming velocity $U(t)$, which consists of the quasi-steady term given by (2.4), plus another oscillatory term with zero mean, plus a decaying term for motions started from rest. The new oscillatory term may be large compared with the quasi-steady term if S is large, but has no effect on the mean swimming speed. If the authors had included the (small) convective inertia and taken their calculation to second order in amplitude, they could have found a significant difference between the predicted mean swimming speed and that calculated by Blake (1971).

The pairwise interaction of two unsteady squirmers has been studied by Giacché & Ishikawa (2010) and by Delmotte *et al.* (2015). Inertia was not included so the flow field is quasi-steady at each instant, and the studies were restricted to coplanar trajectories. Giacché & Ishikawa (2010) took the two squirmers to have identical tangential surface displacements (4.2b), with $\beta_n(t) = 0$ for $n > 3$ and

$$\beta_1(t) = b_1 \sin(\sigma t + \chi), \quad \beta_2(t) = b_2 \cos(\sigma t + \chi), \quad \beta_3(t) = b_3 \sin(\sigma t + \chi); \quad (4.16)$$

the only difference between the two squirmers was that the value of χ could be different. These particular displacement functions are the same as those chosen by Magar & Pedley (2005) and by Wang & Ardekani (2012) to represent isolated unsteady squirmers; different choices of the constants b_j permit *hovering* ($\bar{U} = 0$) and *neutral swimming* ($B_2 = 0$) as well as general *streaming*. Giacché & Ishikawa (2010) evaluated the flow fields numerically, using the same boundary element method as Ishikawa *et al.* (2006). They characterised the importance of unsteadiness by calculating the difference in the scattering angle, after a close encounter, between steady and unsteady squirmers with the same mean swimming speeds. They examined two of the cases used by Ishikawa *et al.* (2006) for steady squirmers: in one case the squirmers were initially oriented in opposite directions, on paths a distance a apart, and in the other case the initial orientations were perpendicular and, if the spheres moved in straight lines at constant speed, they would collide. The biggest effect on the scattering angle occurred when the phases of the two squirmers were different. Delmotte *et al.* (2015) conducted a similar study, using the force coupling method, and with different functions of time for the tangential velocity on the squirmer surface, including terms with frequencies σ , 2σ and 3σ (compare (4.16)) in order to simulate the data of Guasto *et al.* (2010) on *Chlamydomonas reinhardtii*. They also found that the effect on the trajectories was quite small, but increased as the phase difference between the two squirmers increased. The implication is that unsteadiness can have a significant effect on the near-field hydrodynamics of two swimmers, and therefore that it should not be neglected in multiparticle simulations like those of Ishikawa & Pedley (2007a,b, 2008), Ishikawa *et al.* (2008), Evans *et al.* (2011) and others. Delmotte *et al.* (2015) did conduct simulations of a suspension of many unsteady squirmers with the same frequency and indeed found that the assumed distribution of phases between them had a significant effect on the time course and eventual value of the order parameter $P(t)$ (3.1).

5. Conclusion

A spherical squirmer, especially a steady one, is a highly idealised model of any real micro-organism, with the possible exception of *Volvox*. The advantage, especially of steady squirmers with only tangential, not radial, velocities on the spherical surface, is that boundary conditions can be applied precisely, with the result that all properties of the fluid flow and nutrient concentration distribution around an individual squirmer can be derived analytically, or at least with a precise computation. It follows that computations of the macroscopic diffusive and rheological properties of suspensions of many squirmers can be performed with confidence. However, if we set ourselves the long-term goal of developing (approximate) continuum models for non-dilute suspensions of swimming micro-organisms, a number of important questions remain unanswered. (a) The diffusive properties of a suspension, such as: how should the dispersion of interacting squirmers be described when the time- or length-scales of the phenomena of interest are not much larger than the time between ‘collisions’ or the mean free path of a squirmer? The non-uniform suspension described in Section 3.3 needs to be supplemented with a range of further studies with larger macroscopic length scales. (b) What are the general rheological properties of suspensions of bottom-heavy squirmers, for which only a small part of parameter space has

yet been examined? (c) How should noise in the environment or possibly small but random differences between the properties of squirmers in the suspension, such as their radius or squirming parameters B_j , be incorporated into the model?

The last of these questions leads to the main disadvantage of the spherical squirmer model: real biological micro-organisms (apart from *Volvox*) are not spherical and none of them actually squirm. In the case of *Volvox*, one can see how to improve the fluid dynamical description of its locomotion, by using slender-body theory for each individual flagellum and its image in the sphere. As implied above, research on this is currently under way, but it will be a big computation so not many different cases can be computed. Elongated micro-organisms can be modelled as prolate spheroidal squirmers (Kanevsky *et al.*, 2010), so that the steric and hydrodynamic interactions between them can be described precisely, but it will remain a major computational challenge to simulate accurately more than two actual micro-organisms with long flagella, waving or rotating.

Perhaps the most important principle for applied mathematical modellers of swimming micro-organisms to bear in mind is that their objective is to shed light on real phenomena, in biology or microtechnology. It is very easy for a simple model to take on a life of its own, and the more complicated the problem it is used for, the less broad will be its applicability, because of all the additional assumptions and approximations that are required.

Acknowledgement

I would like to give special acknowledgement to those colleagues and former students who performed a lot of the research reviewed here: Douglas Brumley, Takuji Ishikawa and Vanesa Magar. I would also like to thank my current colleagues Raymond Goldstein, Eric Lauga and Yongyun Hwang for their interest, support and enlightening discussions.

REFERENCES

- ACRIVOS, A. & TAYLOR, T. D. (1962) Heat and mass transfer from single spheres in Stokes flow. *Phys. Fluids*, **5**, 387–394.
- ALARCON, F. & PAGONABARRAGA, I. (2013) Spontaneous aggregation and global polar ordering in squirmer suspensions. *J. Mol. Liq.*, **185**, 56–61.
- ANDERSON, J. L. & PRIEVE, D. C. (1991) Diffusiophoresis caused by gradients of strongly adsorbing solutes. *Langmuir*, **7**, 403–406.
- ARANSON, I. S., SOKOLOV, A., KESSLER, J. O. & GOLDSTEIN, R. E. (2007) A model for dynamical coherence in thin films of self-propelled microorganisms. *Phys. Rev. E*, **75**, 040901.
- BATCHELOR, G. K. (1970) The stress system in a suspension of force-free particles. *J. Fluid Mech.*, **41**, 545–570.
- BATCHELOR, G. K. (1977) The effect of Brownian motion on the bulk stress in a suspension of spherical particles. *J. Fluid Mech.*, **83**, 97–117.
- BATCHELOR, G. K. & GREEN, J. T. (1972a) The determination of the bulk stress in a suspension of spherical particles to order c^2 . *J. Fluid Mech.*, **56**, 401–427.
- BATCHELOR, G. K. & GREEN, J. T. (1972b) The hydrodynamic interaction of two small freely-moving spheres in a linear flow field. *J. Fluid Mech.*, **56**, 375–400.
- BEES, M. A. & HILL, N. A. (1997) Wavelengths of bioconvection patterns. *J. Exp. Biol.*, **200**, 1515–1526.
- BEES, M. A. & HILL, N. A. (1998) Linear bioconvection in a suspension of randomly swimming, gyrotactic micro-organisms. *Phys. Fluids*, **10**(8), 1864–1881.
- BEES, M. A. & HILL, N. A. (1999) Non-linear bioconvection in a deep suspension of gyrotactic swimming micro-organisms. *J. Math. Biol.*, **38**, 135–168.
- BERG, H. C. (2004) *E. coli in Motion*. New York, Springer.

- BERG, H. C. & PURCELL, E. M. (1977) Physics of chemoreception. *Biophys. J.*, **20**, 193–219.
- BLAKE, J. R. (1971) A spherical envelope approach to ciliary propulsion. *J. Fluid Mech.*, **46**, 199–208.
- BRENNEN, C. & WINET, H. (1977) Fluid mechanics of propulsion by cilia and flagella. *Annu. Rev. Fluid Mech.*, **9**, 339–398.
- BRUMLEY, D. R. (2013) Hydrodynamics of swimming micro-organisms. *Ph.D. Thesis*, University of Cambridge.
- BRUMLEY, D. R., POLIN, M., PEDLEY, T. J. & GOLDSTEIN, R. E. (2012) Hydrodynamic synchronization and metachronal waves on the surface of the colonial alga *Volvox carteri*. *Phys. Rev. Lett.*, **109**, 268102.
- CHILDRESS, S., LEVANDOWSKY, M. & SPIEGEL, E. A. (1975) Pattern formation in a suspension of swimming micro-organisms. *J. Fluid Mech.*, **69**, 591–613.
- CISNEROS, L. H., CORTEZ, R., DOMBROWSKI, C., GOLDSTEIN, R. E. & KESSLER, J. O. (2007) Fluid dynamics of self-propelled micro-organisms, from individuals to concentrated populations. *Exp. Fluids*, **43**, 737–753.
- DELMOTTE, B., KEAVNEY, E., PLOURABOUE, F. & CLIMENT, E. (2015) Large-scale simulation of steady and time-dependent active suspensions with the force-coupling method. *J. Comput. Phys.*, **302**, 524–547.
- DOMBROWSKI, C., CISNEROS, L., CHATKAEW, S., GOLDSTEIN, R. E. & KESSLER, J. O. (2004) Self-concentration and large-scale coherence in bacterial dynamics. *Phys. Rev. Lett.*, **93**, 098103.
- DOOSTMOHAMMADI, A., STOCKER, R. & ARDEKANI, A. M. (2012) Low-Reynolds-number swimming at pycnoclines. *Proc. Natl Acad. Sci. U. S. A.*, **109**, 3856–3861.
- DRESCHER, K., LEPTOS, K. C., TUVAL, I., ISHIKAWA, T., PEDLEY, T. J. & GOLDSTEIN, R. E. (2009) Dancing *Volvox*: hydrodynamic bound states of swimming algae. *Phys. Rev. Lett.*, **102**, 168101.
- ECKHARDT, B. & ZAMMERT, S. (2012) Non-normal tracer diffusion from stirring by swimming microorganisms. *Eur. Phys. J. E.*, **35**, 96.
- EINSTEIN, A. (1906) Eine neue Bestimmung der Moleküldimensionen. *Ann. Phys.*, **19**, 289–306.
- EVANS, A. A., ISHIKAWA, T., YAMAGUCHI, T. & LAUGA, E. (2011) Orientational order in concentrated suspensions of spherical microswimmers. *Phys. Fluids*, **23**, 111702.
- EZHILAN, B., SHELLEY, M. J. & SAINTILLAN, D. (2013) Instabilities and nonlinear dynamics of concentrated active suspensions. *Phys. Fluids*, **25**, 070697.
- FELDERHOF, B. U. & JONES, R. B. (1994) Small-amplitude swimming of a sphere. *Physica A*, **202**, 119–144.
- FELDERHOF, B. U. & JONES, R. B. (2016) Stokesian swimming of a sphere at low Reynolds number. ArXiv [physics.fluid-dyn], 1602, 01249.
- GHOSE, S. & ADHIKARI, R. (2014) Irreducible representations of oscillatory and swirling flows in active soft matter. *Phys. Rev. Lett.*, **112**, 118102.
- GIACCHE, D. & ISHIKAWA, T. (2010) Hydrodynamic interaction of two unsteady model microorganisms. *J. Theor. Biol.*, **267**, 252–263.
- GOLDSTEIN, R. E. (2015) Green algae as model organisms for biological fluid dynamics. *Annu. Rev. Fluid Mech.*, **47**, 343–375.
- GOLESTANIAN, R., LIVERPOOL, T. B. & AJDARI, A. (2005) Propulsion of a molecular machine by asymmetric distribution of reaction products. *Phys. Rev. Lett.*, **94**, 220801.
- GUASTO, J. S., JOHNSON, K. A. & GOLLUB, J. P. (2010) Oscillatory flows induced by micro-organisms swimming in two dimensions. *Phys. Rev. Lett.*, **105**, 168102.
- GUASTO, J. S., RUSCONI, R. & STOCKER, R. (2012) Fluid mechanics of planktonic microorganisms. *Annu. Rev. Fluid Mech.*, **44**, 373–400.
- HAINES, B. M., SOKOLOV, A., ARANSON, I. S., BERYLAND, L. & KARPEEV, D. A. (2009) Three-dimensional model for the effective viscosity of bacterial suspensions. *Phys. Rev. E*, **80**, 041922.
- HATWALNE, Y., RAMASWAMY, S., RAO, M. & SIMHA, R. A. (2004) Rheology of active-particle suspensions. *Phys. Rev. Lett.*, **92**, 118101.
- HILL, N. A. & PEDLEY, T. J. (2005) Bioconvection. *Fluid Dyn. Res.*, **37**, 1–20.
- HILLESDON, A. J. & PEDLEY, T. J. (1996) Bioconvection in suspensions of oxytactic bacteria: linear theory. *J. Fluid Mech.*, **324**, 223–259.
- HINCH, E. J. & LEAL, L. G. (1972) The effect of Brownian motion on the rheological properties of a suspension of non-spherical particles. *J. Fluid Mech.*, **52**, 683–712.

- ISHIKAWA, T., LOCSEI, J. T. & PEDLEY, T. J. (2008) Development of coherent structures in concentrated suspensions of swimming model micro-organisms. *J. Fluid Mech.*, **615**, 401–431.
- ISHIKAWA, T., LOCSEI, J. T. & PEDLEY, T. J. (2010) Fluid particle diffusion in a semi-dilute suspension of model micro-organisms. *Phys. Rev. E*, **82**, 021408.
- ISHIKAWA, T. & PEDLEY, T. J. (2007a) Diffusion of swimming model micro-organisms in a semi-dilute suspension. *J. Fluid Mech.*, **588**, 437–462.
- ISHIKAWA, T. & PEDLEY, T. J. (2007b) The rheology of a semi-dilute suspension of swimming model micro-organisms. *J. Fluid Mech.*, **588**, 399–435.
- ISHIKAWA, T. & PEDLEY, T. J. (2008) Coherent structures in monolayers of swimming particles. *Phys. Rev. Lett.*, **100**, 088103.
- ISHIKAWA, T. & PEDLEY, T. J. (2014) Dispersion of model micro-organisms swimming in a non-uniform suspension. *Phys. Rev. E*, **90**, 033008.
- ISHIKAWA, T., SIMMONDS, M. P. & PEDLEY, T. J. (2006) Hydrodynamic interaction of two swimming model micro-organisms. *J. Fluid Mech.*, **568**, 119–160.
- ISHIMOTO, K. & GAFFNEY, E. A. (2013) Squirm dynamics near a boundary. *Phys. Rev. E*, **88**, 062702.
- KANEVSKY, A., SHELLY, M. J. & TORNBERG, A.-K. (2010) Modeling simple locomotors in Stokes flow. *J. Comput. Phys.*, **229**, 958–977.
- KESSLER, J. O. (1985) Co-operative and concentrative phenomena of swimming microorganisms. *Contemp. Phys.*, **26**, 147–166.
- KESSLER, J. O. (1986) Individual and collective dynamics of swimming cells. *J. Fluid Mech.*, **173**, 191–205.
- KESSLER, J. O., HOELZER, M. A., PEDLEY, T. J. & HILL, N. A. (1994) Functional patterns of swimming bacteria. *Mechanics and Physiology of Animal Swimming* (Maddock, L., Bone, Q. & Rayner, J. M. V., eds). Cambridge, Cambridge University Press, pp. 3–12.
- Koch, D. L. & Subramanian, G. (2011) Collective hydrodynamics of swimming micro-organisms: living fluids. *Annu. Rev. Fluid Mech.*, **43**, 637–659.
- LAMBERT, R. A., PICANO, F., BREUGEM, W.-P. & BRANDT, L. (2013) Active suspensions in thin films: nutrient uptake and swimmer motion. *J. Fluid Mech.*, **733**, 528–557.
- LAUGA, E. & POWERS, T. R. (2009) The hydrodynamics of swimming microorganisms. *Rep. Prog. Phys.*, **72**, 096601.
- LEPTOS, K. C., GUASTO, J. S., GOLLUB, J. P., PESCI, A. I. & GOLDSTEIN, R. E. (2009) Dynamics of enhanced tracer diffusion in suspensions of swimming eukaryotic microorganisms. *Phys. Rev. Lett.*, **103**, 198103.
- LI, G.-J. & ARDEKANI, A. M. (2014) Hydrodynamic interaction of microswimmers near a wall. *Phys. Rev. E*, **90**, 013010.
- LIGHTHILL, J. (1975) *Mathematical Biofluidynamics*. Philadelphia: SIAM.
- LIGHTHILL, M. J. (1950) Contributions to the theory of heat transfer through a laminar boundary layer. *Proc. R. Soc. Lond. A*, **202**, 359–377.
- LIGHTHILL, M. J. (1952) On the squirming motion of nearly spherical deformable bodies through liquids at very small Reynolds numbers. *Commun. Pure Appl. Math.*, **5**(2), 109–118.
- LIN, Z., THIFFEAULT, J.-L. & CHILDRESS, S. (2011) Stirring by squirmers. *J. Fluid Mech.*, **669**, 167–177.
- LOMHOLT, S. & MAXEY, M. (2003) Force-coupling method for particulate two-phase flow: Stokes flow. *J. Comput. Phys.*, **184**, 381–405.
- MAGAR, V., GOTO, T. & PEDLEY, T. J. (2003) Nutrient uptake by a self-propelled steady squirmer. *Q. J. Mech. Appl. Math.*, **56**, 65–91.
- MAGAR, V. & PEDLEY, T. J. (2005) Average nutrient uptake by a self-propelled unsteady squirmer. *J. Fluid Mech.*, **539**, 93–112.
- MATAS-NAVARRO, R., GOLESTANIAN, R., LIVERPOOL, T. B. & FIELDING, S. M. (2014) Hydrodynamic suppression of phase separation in active suspensions. *Phys. Rev. E*, **90**, 032304.
- MAVRAMATIS, K., YASAWONG, M., CHERTKOV, O., LAPIDUS, A., LUCAS, S., NOLAN, M., DEL RIO, T. G., TICE, H., CHENG, J.-F., PITLUCK, S., LIOLIOS, K., IVANOVA, N., TAPIA, R., HAN, C., BRUCE, D., GOODWIN, L., PATI, A., CHEN, A., PALANIAPPAN, K., LAND, M., HAUSER, L., CHANG, Y.-J., JEFFRIES, C. D., DETTER, J. C., ROHDE, M., BRAMBILLA, E., SPRING, S., GÖKER, M., SIKORSKI, J., WOYKE, T., BRISTOW, J., EISEN, J. A., MARKOWITZ,

- V., HUGENHOLTZ, P., KLENK, H.-P. & KYRPIDES, N. C. (2010) Complete genome sequence of Spirochaeta smaragdinae type strain (SEBR 4228T). *Stand Genomic Sci.*, **3**, 136–144.
- MAXEY, M. & PATEL, B. (2001) Localized force representations for particles sedimenting in Stokes flow. *Int. J. Multiph. Flow*, **27**, 1603–1626.
- METCALFE, A. M. & PEDLEY, T. J. (1998) Bacterial bioconvection: weakly nonlinear theory for pattern selection. *J. Fluid Mech.*, **370**, 249–270.
- METCALFE, A. M. & PEDLEY, T. J. (2001) Falling plumes in bacterial bioconvection. *J. Fluid Mech.*, **445**, 121–149.
- MICHELIN, S. & LAUGA, E. (2010) Efficiency optimization and symmetry-breaking in a model of ciliary locomotion. *Phys. Fluids*, **22**, 111901.
- MICHELIN, S. & LAUGA, E. (2011) Optimal feeding is optimal swimming for all Péclet numbers. *Phys. Fluids*, **23**, 101901.
- MICHELIN, S. & LAUGA, E. (2013) Unsteady feeding and optimal strokes of model ciliates. *J. Fluid Mech.*, **715**, 1–31.
- MICHELIN, S., LAUGA, E. & BARTOLO, D. (2013) Spontaneous autophoretic motion of isotropic particles. *Phys. Fluids*, **25**, 061701.
- PAK, O. S. & LAUGA, E. (2014) Generalized squirming motion of a sphere. *J. Eng. Math.*, **88**, 1–28.
- PEDLEY, T. J. (2010a) Collective behaviour of swimming micro-organisms. *Exp. Mech.*, **50**, 1293–1301.
- PEDLEY, T. J. (2010b) Instability of uniform microorganism suspensions revisited. *J. Fluid Mech.*, **647**, 335–359.
- PEDLEY, T. J., BRUMLEY, D. R. & GOLDSTEIN, R. E. (2016) Squirmers with swirl—a model for *Volvox* swimming. *J. Fluid Mech.*, **798**, 165–186.
- PEDLEY, T. J. & KESSLER, J. O. (1992) Hydrodynamic phenomena in suspensions of swimming micro-organisms. *Annu. Rev. Fluid Mech.*, **24**, 313–358.
- PLATT, J. R. (1961) ‘Bioconvection patterns’ in cultures of free-swimming organisms. *Science*, **133**, 1766–1767.
- PUSHKIN, D. O., SHUM, H. & YEOMANS, J. M. (2013) Fluid transport by individual microswimmers. *J. Fluid Mech.*, **726**, 5–25.
- RAFAI, S., JIBUTI, L. & PEYLA, P. (2010) Effective viscosity of microswimmer suspensions. *Phys. Rev. Lett.*, **104**, 098102.
- RÜFFER, U. & NULTSCH, W. (1985) High-speed cinematographic analysis of the movement of *Chlamydomonas*. *Cell Motil.*, **5**, 251–263.
- SAINTILLAN, D. (2010) The dilute rheology of swimming suspensions: a simple kinetic model. *Exp. Mech.*, **50**, 1275–1281.
- SAINTILLAN, D. & SHELLEY, M. J. (2008) Instabilities, pattern formation, and mixing in active particle suspensions. *Phys. Fluids*, **20**, 123304.
- SAINTILLAN, D. & SHELLEY, M. J. (2012) Emergence of coherent structures and large-scale flows in motile suspensions. *J. R. Soc. Interface*, **9**, 571–585.
- SHORT, M. B., SOLARI, C. A., GANGULY, S., POWERS, T. R., KESSLER, J. O. & GOLDSTEIN, R. E. (2006) Flows driven by flagella of multicellular organisms enhance long-range molecular transport. *Proc. Natl Acad. Sci. U. S. A.*, **103**, 8315–8319.
- SIMHA, R. A. & RAMASWAMY, S. (2002) Hydrodynamic fluctuations and instabilities in ordered suspensions of self-propelled particles. *Phys. Rev. Lett.*, **89**, 058101.
- SLEIGH, M. A. (1962) *The Biology of Cilia and Flagella*. Oxford, Pergamon Press.
- SOKOLOV, A. & ARANSON, I. S. (2009) Reduction of viscosity in suspension of swimming bacteria. *Phys. Rev. Lett.*, **103**, 148101.
- SOKOLOV, A. & ARANSON, I. S. (2012) Physical properties of collective motion in suspensions of bacteria. *Phys. Rev. Lett.*, **109**, 248109.
- STONE, H. A. & SAMUEL, A. D. T. (1996) Propulsion of microorganisms by surface distortions. *Phys. Rev. Lett.*, **77**, 4102–4104.
- TAYLOR, G. I. (1951) Analysis of the swimming of microscopic organisms. *Proc. R. Soc. Lond. A*, **209**, 447–461.
- THIFFEAULT, J.-L. & CHILDRESS, S. (2010) Stirring by swimming bodies. *Phys. Lett. A*, **374**, 3487–3490.

- THUTUPALLI, S., SEEMANN, R. & S, H. (2011) Swarming behaviour of simple model squirmers. *New J. Phys.*, **13**, 073021.
- TRIPOS (1986) *Mathematical Tripos, Part II, Paper 4*. University of Cambridge.
- Wager, H. (1911) On the effect of gravity upon the movements and aggregation of *Euglena viridis* and other micro-organisms. *Philos. Trans. R. Soc. Lond. B*, **201**, 333–390.
- WANG, S. & ARDEKANI, A. M. (2012) Unsteady swimming of small organisms. *J. Fluid Mech.*, **702**, 286–297.
- WATERBURY, J. B., WILLEY, J. M., FRANKS, D. G., VALOIS, F. W. & WATSON, S. W. (1985) A cyanobacterium capable of swimming motility. *Science*, **230**, 74–76.
- WU, X. L. & LIBCHABER, A. (2000) Particle diffusion in a quasi-two-dimensional bacterial bath. *Phys. Rev. Lett.*, **84**, 3017–3020.
- ZHU, L., LAUGA, E. & BRANDT, L. (2013) Low-Reynolds number swimming in a capillary tube. *J. Fluid Mech.*, **726**, 285–311.
- ZÖTTL, A. & STARK, H. (2014) Hydrodynamics determines collective motion and phase behaviour of active colloids in quasi-two-dimensional confinement. *Phys. Rev. Lett.*, **112**, 118101.